A Biologically Inspired Compound-Eye Detector Array—Part I: Modeling and Fundamental Limits

Zhi Liu, *Student Member, IEEE*, Arye Nehorai, *Fellow, IEEE*, and Eytan Paldi, *Member, IEEE*

***Abstract*—This is the first part of a two-part paper. In this paper, we propose a detector array for detecting and localizing sources that emit particles including photons, neutrons, or charged particles. The array consists of multiple "eyelets." Each eyelet has a conical module with a lens on its top and an inner subarray containing multiple particle detectors. The array configuration is inspired by and generalizes the biological compound eye: it is spherically shaped and has a larger number of detectors in each individual eyelet. Potential applications of this biomimetic array include artificial vision in medicine (e.g., artificial eyes for the blind) or robotics (e.g., for industry or space missions), astronomy and astrophysics, security (e.g., for radioactive materials), and particle communications. In this part, we assume Poisson distribution for each detector's measurement within the observation time window. Then we construct a general parametric model for the detection rate of the Poisson-distributed measurements illustrated by a circular Gaussian lens-shaping function (LSF) approximation, which is commonly used in optical and biological disciplines. To illustrate how this "prototype" model fits practical cases, we apply it to an example of localizing a candle from 20 miles away and estimating the parameters under this circumstance. In addition, we also discuss the hardware setup and performance measure of the proposed array, as well as its fundamental constraints. Part I forms the theoretical basis for Part II, in which we analyze the performance of the array, both analytically and numerically.**

***Index Terms*—Artificial compound eye, biologically inspired, biomimetics, eyelet, fundamental limits, lens, mean-square angular error, modeling, particle communication, particle detector array, particle source localization, weighted direction estimator.**

I. Introduction

In Part I of our paper, we propose a novel detector array for detecting and localizing particle-emitting sources. The array consists of multiple "eyelets," each having a conical module with a lens on its top and an inner subarray containing a large number of small particle detectors (for different types of particle detectors, see e.g., [1]–[4]). The eyelets can be used to detect uncharged particles such as photons and neutrons. For the case of visible-light sources, this array configuration is a generalization of the biological compound eye, being spherically shaped and having a larger number of detectors in each individual eyelet. Compared with most existing optical sensor arrays (e.g., planar CCD or CMOS sensor arrays in digital cameras), the proposed sensor array has a larger field of view (because of its spherical shape) and higher sensitivity to the source direction (because of multiple eyelets). In other words, the proposed array combines the advantages of the biological compound eye (large field of view) and of human eyes (high spatial resolution). Moreover, the size of the spherical array is compact, compared with other distributed sensor arrays (e.g., distributed antenna arrays for localizing EM sources).

This work extends our previous work on directional detector arrays, in which we introduced several detector arrays, computed their performance bounds for source localization [5], and proposed a detection algorithm to determine the presence of a far-field particle source [6]. The current extensions include the introduction of multiple eyelets, lenses, and subarrays. Compared with the arrays with projection response to the source direction in [5] and [6], the proposed array with lenses on top of subarrays possesses a sharper response function and one that is adjustable, and hence the angular resolution is increased markedly. In this two-part paper, we extend our earlier results in [7], where we briefly introduced the configuration of the proposed array, and in [8], where we analyzed the performance of the array numerically. We expand our work in [7] and [8], by generalizing the mathematical model and adding new analytical and numerical results.

A. Motivation and Applications

This work is motivated by the need for sensitive particle sensors in applications such as artificial vision, which can be important in robotics (see, e.g., [9]) or medicine (e.g., artificial eyes for the blind); security, where the detection of radioactive materials is needed (e.g., in verifying compliance with nuclear nonproliferation treaties); and astronomy assisted (e.g., estimation of orientation and angular velocity with respect to the stars for satellites and space vehicles). Potential applications also include "particle communication." Different types of particles in potential applications are listed in Table I. Notably, an artificial compound eye that mimics a biological compound eye anatomically as well as functionally was recently built [10]. This achievement indicates that the array configuration proposed in this paper is not merely a "thought experiment" but is a potentially practical one that may have wide impact in the above areas.

Manuscript received October 27, 2007; accepted November 26, 2008. First published February 06, 2009; current version published April 15, 2009. The associate editor coordinating the review of this manuscript and approving it for publication was Prof. Mounir Ghogho. This work was supported by the AFOSR Grant FA9550-05-1-0018 and the National Science Foundation Grants CCR-0330342 and CCF-0630734.

Z. Liu is with OSIsoft, Inc., San Leandro, CA 94577 USA (e-mail: zliu@osisoft.com).

A. Nehorai is with the Department of Electrical and Systems Engineering, Washington University in St. Louis, St. Louis, MO 63130 USA (e-mail: nehorai@ese.wustl.edu).

E. Paldi is with the Department of Mathematics, Israel Institute of Technology, Technion City, Haifa 32000, Israel (e-mail: epmath@techunix.technion.ac.il).

Color versions of one or more of the figures in this paper are available online at http://ieeexplore.ieee.org.

Digital Object Identifier 10.1109/TSP.2009.2014699

TABLE I
PARTICLES IN DIFFERENT APPLICATIONS

Applications	Sources of interest	Particles including (but not limited to)
artificial vision	optical	infrared and visible photons
astronomy, astrophysics	cosmic	photons, other cosmic particles[1]
security	optical, radioactive	photons, neutrons, charged particles[2]
particle communication	optical, radioactive	photons, other particles[1]

[1]The choice of particles and detectors depends on the specific application.

[2]Charged particles are subject to scattering.

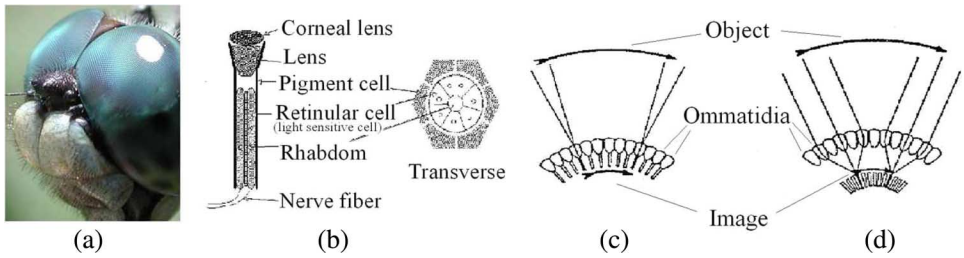

Fig. 1. (a) Dragonfly's compound eye; (b) anatomical cross section of a compound eye and an ommatidium; (c) optics of an apposition compound eye; and (d) optics of a superposition compound eye.

Remark 1.1: Although we used visible photons in the analysis of this paper, the proposed array and the mathematical/practical model apply to all the types of particles listed in Table I.

B. Outline of This Part

This part focuses mainly on modeling the array's behavior in localizing particle sources, both statistically and physically. First, we assume a Poisson distribution for each detector's measurement within the observation time window. Then, we construct a general parametric model for the detection rate of the Poisson-distributed measurements illustrated by a circular Gaussian lens-shaping function (LSF) approximation, which is widely used in optical and biological disciplines. To illustrate how this "prototype" model fits in practical cases, we apply it to an example of localizing a candle from 20 miles away and estimate the parameters under this circumstance. In addition, we also discuss the hardware setup of the proposed array and the fundamental constraints on the array variables. Finally, we introduce a performance measure of the array and analyze its fundamental limitations.

Part I forms the analytical basis for Part II, in which we will analytically and numerically analyze the performance of the array. Part I is organized as follows: in Section II, we briefly describe the optical properties of different types of compound eyes and compare them with the proposed array; in Section III and Section IV, we introduce the general mathematical measurement model and the statistical measurement model for the array, respectively; in Section V, we present an example to show how the model can be used in practice; in Section VI, we discuss the hardware setup and fundamental limits of the array variables; in Section VII, we introduce the array's performance measure and analyze its fundamental bounds; in Section VIII, we summarize this work.

II. BIOLOGICAL COMPOUND EYES AND THE PROPOSED ARRAY

We briefly describe the optical properties of biological compound eyes and introduce the configuration of the proposed array.

A. Biological Compound Eyes

A compound eye is a visual organ found in certain arthropods (some insects and crustaceans), as shown in Fig. 1(a). It usually contains multiple "ommatidia," each consisting of a lens and a rhabdom; see Fig. 1(b). In contrast to the single-aperture eyes of vertebrates, compound eyes have no central lens or retina. From an optical viewpoint, compound eyes can be classified into two fundamental categories [11]: *apposition* and *superposition*.

As the commonest type and possibly the ancestor of the others, an *apposition eye* has its rhabdoms receiving light only from their "own" corneal facets [12]. This eye consists of an array of up to 30 000 individual ommatidia, each containing a lens on the top with a cluster of (usually seven or eight) photoreceptor cells inside, which form a single photosensitive light-guiding rod, or rhabdom [13]. In other words, the ommatidia work as optically isolated units in these eyes, as shown in Fig. 1(c). In these eyes, each ommatidium collects light rays coming from a small part of the object and forms a small image of that part on its distal tip. Combination of all these small images creates a complete image of the whole object.

In contrast, *superposition eyes* have the characteristic that the ommatidia are not optically isolated. The term "superposition" refers to the fact that contributions from many optical elements are superimposed in the image plane [11]. In these eyes, each rhabdom senses light from a large number of corneal lenses, and each facet forms an image that extends over many rhabdoms [see Fig. 1(d)]. The superposition mechanism combines the small images of each rhabdom into a single image of the object.

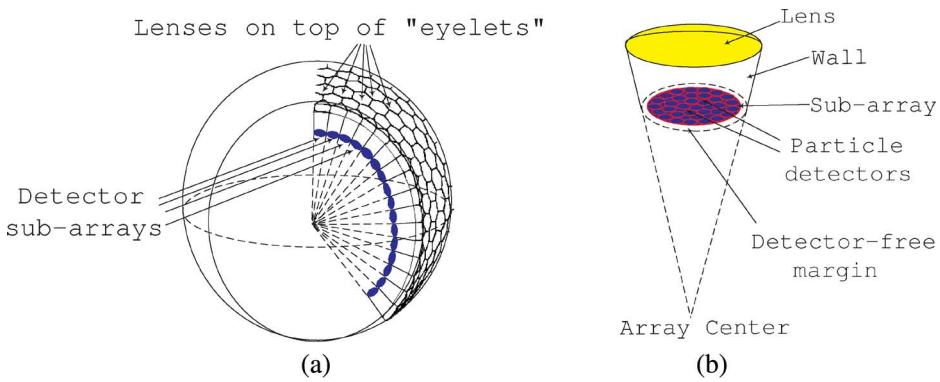

Fig. 2. (a) Cross section of a segment of the proposed array and (b) schematic description of each eyelet, with a lens on top of a conical module and an inside subarray of detectors.

TABLE II
TERMINOLOGY USED FOR THE BIOLOGICAL COMPOUND EYE AND THE PROPOSED ARRAY

Terms for the biological eye	Terms for the proposed array
ommatidium	eyelet
lens, corneal lens	lens
rhabdom	sub-array
photoreceptor cell (visual cell, rhabdomere)	detector
pigment cell	wall of the conical module in the eyelet

Compared with single-aperture eyes, compound eyes have a much wider field-of-view (FOV), better capability to detect moving objects, and higher sensitivity to light intensity. Moreover, a compound eye may perform the function of multiple arrays simultaneously, each having different spectral responses, polarization sensitivity, integration times, or adaption organisms [12]. However, because of the tiny aperture size of each corneal lens and small number of detectors in each ommatidium, the diffraction effect of light limits the spatial resolution to about 1, yielding an image roughly 100 times coarser than that of human eyes.

B. The Proposed Array

The proposed array is spherical and contains multiple optically isolated eyelets [see Fig. 2(a)] inspired by an apposition compound eye. The reasons for choosing the apposition compound eye as the "template" include its simplicity of structure and popularity in nature. As shown in Fig. 2(b), each eyelet has a conical module with a lens on top and a subarray inside containing a large number of small particle detectors. Between the detectors and the edge of the conical module, there is a "detector-free margin" whose purpose is to make negligible the distortion of the lens-shaping function due to scattering of particles near the cone's edge. Under the focusing effect of the lens, the incident particles form an intensity distribution on the subarray, inducing a random measurement at each detector. These measurements contain information about the source direction, which can be extracted using statistical methods.

We configure the proposed array with two major modifications on the apposition compound eye: i) providing the proposed array with a $4\pi\text{rad}^2$ FOV by a complete spherical shape (in practice the FOV may be less if mounting is considered), and ii) allowing a larger number of detectors in each subarray. Both modifications, as shown in the analysis below, remarkably improve the array performance. To further understand the similarities between the biological compound eye and the proposed array, we compare the terminology used for both structures in Table II.

III. General Mathematical Measurement Model

We consider several remote point sources whose intensities in the array vicinity are assumed to be homogeneous. The measurements of the array are particle counts of all detectors within an observation time window containing information about the source direction of interest. In order to analyze the array performance, we construct a model for these measurements.

A. Concepts, Notations, Assumptions, and Transfer Function Derivation

In Appendix D, we introduce several definitions, notations, and assumptions that are needed for the derivation of the transfer function for the general model. Based on those definitions, we derive the general model of the proposed array below.

B. Orthonormal Basis Expansion for the Array Transfer Function

Since the transfer function $H(d; E, \boldsymbol{u})$ for each detector d is (from a physical consideration) arbitrarily closely approximated through its truncation by a threshold energy, we may assume that it vanishes outside some *finite* energy band $[E_1, E_2]$. Let $\phi_k(E)$, $k \geq 1$ be any given *complete* system of orthonormal basis functions on $[E_1, E_2]$, the transfer function can be expanded according to this basis with corresponding coefficients $a_k(d; \boldsymbol{u})$ and converge in $L^2[E_1, E_2]$ to the transfer function. In this sense, the dependencies of the transfer function on E and $\boldsymbol{u}$ are separated. The coefficients $a_k(d; \boldsymbol{u})$ play the physical role of the detector cross section for the function $\phi_k(E)$. Since this expansion holds for *any* given complete orthonormal system of basis functions, it is of importance to find an *optimal*

orthonormal basis functions for the transfer function. We find this optimal basis functions using a (continuous) version of singular value decomposition (SVD) for integral kernels.

C. Optimization of the Orthonormal Basis Functions and LPG Functions Approximation

The optimal basis functions problem is to find an orthonormal basis function such that the truncation of the transfer function expansion after any given number of terms should give the best L^2 approximation to the transfer function over the energy-direction space (EDS). The construction of the optimal basis and its proof are very similar to the discrete kernel (i.e., matrix) case. So we give below only the construction.

Define the integral kernel

$$K(E,E') = \int_{\mathrm{US}} H(E,\boldsymbol{u})H(E',\boldsymbol{u})\mathrm{d}m(\boldsymbol{u})$$

where US denotes the unit sphere. It is easy to verify that the kernel K is well defined over the square $[E_1,E_2]^2$, nonnegative, symmetric and sufficiently smooth.

This kernel induces a *compact* integral operator from $L^2[E_1,E_2]$ to itself which is self-adjoint and has a complete orthonormal eigensystem of sufficiently smooth eigenfunctions. The corresponding eigenfunctions $\phi_k(E)$ arranged according to decreasing eigenvalues are the desired optimal basis functions. It is known[1] (from classical theory of Fredholm integral equations) that each eigenvalue has a *finite* dimensional eigenspace (spanned by finitely many eigenfunctions) and each simple eigenvalue *uniquely* determine its eigenfunction (i.e., its one-dimensional eigenspace). Moreover, it follows that for the optimal basis functions, the corresponding coefficients $a_k(\boldsymbol{u})$ of the transfer function are orthogonal as well (over the US).

If the transfer function is strictly positive (in fact, if $K(E,E')$ is strictly positive), a continuous analog of the Perron–Frobenius theorem[2] (for nonnegative matrices) holds for the kernel $K(E,E')$ as well—implying that the first eigenfunction (the most important one) is uniquely defined and its corresponding coefficient $a_1(\boldsymbol{u})$ is *positive* over the US. Since the coefficients $a_k(\boldsymbol{u})$ are orthogonal over the US, it follows that for $k \geq 2$ all the coefficients $a_k(\boldsymbol{u})$ must change signs over the US. Thus, the first coefficient $a_1(\boldsymbol{u})$ is the *only one* that is positive over the US! This implies the importance of this coefficient which gives the best rank-1 approximation of $H(E;\boldsymbol{u})$ by $a_1(\boldsymbol{u})\phi_1(E)$. This rank-1 approximation may serve to define the associate direction $\boldsymbol{u}$ for each detector (independently of E). If from some physical reason, the dependence of the transfer function on E is almost uninfluenced by the direction $\boldsymbol{u}$, then the approximation of the transfer function by a rank-1 kernel is justified.

For a rank-1 kernel approximation, it follows that the frequency dependence $\phi_1(E)$ indicates the detector detection efficiency with respect to energy (hence imply the effective bandwidth $[E_1,E_2]$) whereas $a_1(\boldsymbol{u})$ gives the "lens shaping function" for a point source (as clearly seen by applying the transfer function to the "spherical delta function" representing the directional dependence for point-like source intensity).

[1]See, e.g., [14].

[2]See, e.g., [15].

Finally, as explained in Appendix E, we approximate locally each peak of $a_1(\boldsymbol{u})$ by a Gaussian function (whose associated covariance is determined by the inverse of the Hessian of $\log(a_1(\boldsymbol{u}))$) and multiply it by a spherical polynomial to form a polynomial-Gaussian (PG function) approximant. By taking a linear combination of such PG functions (LPG functions), we can approximate *any* transfer function arbitrarily closely.

Based on Remark D.8, the general modeling for L point-like particle sources and rank-r approximation for the transfer function, takes the form

$$\lambda_{i,j} = \Omega_{i,j}\left[\sum_{k=1}^{r}\sum_{l=1}^{L}\left[a_{i,j,k}(\boldsymbol{u}_l)\mu_{k,l}\right] + \eta_{i,j}\right]$$

where $\lambda_{i,j}$ denotes the detection rate for the i,jth detector. $\Omega_{i,j}$ is the solid angle of the cone of associated directions for the i,jth detector, $a_{i,j,k}(\boldsymbol{u}_l)$ are the above cross section coefficients $a_k(\boldsymbol{u})$ (of the transfer function with respect to the basis function ϕ_k) for the i,jth detector determined for the direction $\boldsymbol{u}=\boldsymbol{u}_l$ of the lth particle source, $\mu_{k,l}$ is the kth coefficient (with respect to the basis function ϕ_k) for the particle intensity $\mu_l(E,\boldsymbol{u})$ for the lth particle source, and $\eta_{i,j}$ are the resulting total noisy detection rate for the i,jth detector. Note that the coefficients $a_{i,j,k}(\boldsymbol{u}_l)$ are approximated as LPG functions of the direction $\boldsymbol{u}_l$ of the lth particle source.

This general modeling has the following specifications: a) rank-r approximation of the transfer function by $\sum_1^r a_k(\boldsymbol{u})\phi_k(E)$; b) rank-1 approximation by $a_1(\boldsymbol{u})\phi_1(E)$; c) LPG approximation of $a_1(\boldsymbol{u})$—especially for multifocal transfer function; d) PG approximation of $a_1(\boldsymbol{u})$; and e) circular Gaussian approximation of $a_1(\boldsymbol{u})$ and uniform approximation for $\phi_1(E)$—this is the simplest or "prototype model" for circular Gaussian transfer function.

IV. Statistical Measurement Model

We consider a single remote point-like source whose intensity in the array vicinity is assumed to be homogeneous and time invariant.[3] The measurements of the array are particle counts of all detectors within the observation time window, containing information for the source direction of interest. In order to analyze the array's performance, first we construct a model for these measurements.

Let M be the number of eyelets in the array and N be the number of detectors in each eyelet on the subarray's detection surface (DS), which is defined as a smooth surface tightly enveloping the detector subarray's physical surface.[4] To obtain isotropic performance (i.e., the array has identical performance in localizing sources over all directions), all eyelets (including lenses, subarrays, and detectors therein) are assumed to have identical physical and geometrical properties. In addition, the locations of the eyelets are assumed to be approximately uniformly distributed over the spherical surface.

[3]The time invariance of the intensity is not really needed and assumed here only for simplicity.

[4]For simplicity, we assume the DS to be planar. Note that the analysis presented below applies also to nonplanar DS cases, for example, the roughly spherical retina in human eyes.

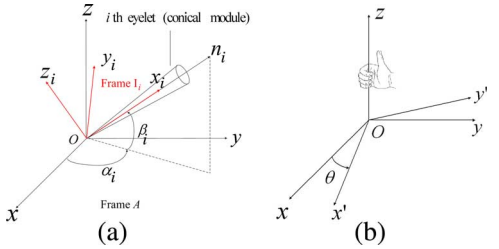

Fig. 3. (a) Reference frames $\mathbf{A}$ and $\mathbf{I}_i$ and (b) right-handed rotation by θ w.r.t. the z axis.

A. Reference Frames

We construct $M+1$ reference frames for the modeling: the array's frame "$\mathbf{A}$" and the ith eyelet's frame "$\mathbf{I}_i$" ($i = 1, \ldots, M$), as shown in Fig. 3(a). For an arbitrary vector $\boldsymbol{v}$ in frame $\mathbf{A}$, let $\boldsymbol{v}_{\mathrm{I}_i}$ be its representation in frame $\mathbf{I}_i$.

In frame $\mathbf{A}$, we choose the origin at the center of the array. Denote the coordinate system as (x, y, z). Let $\boldsymbol{u} = [\cos\phi\cos\psi, \sin\phi\cos\psi, \cos\psi]^T$ be the unit vector along the source direction, where ϕ and ψ are the azimuth and elevation angles, respectively. Denote by $\boldsymbol{u}_i$ as the unit vector along the symmetry axis of the ith eyelet (or the conical module) pointing outward, with α_i and β_i being its azimuth and elevation angles. From the isotropic assignment of the (so-called "balanced design") eyelets, we have $\sum_{i=1}^{M} \boldsymbol{u}_i \approx [0,0,0]^T$.

Reference frame $\mathbf{I}_i$, with its coordinate system denoted as (x_i, y_i, z_i), results from two consecutive right-handed rotations [see Fig. 3(b)] from frame $\mathbf{A}$: first rotate frame $\mathbf{A}$ with respect to the z axis by angle α_i; then rotate the resulting frame with respect to its y axis by angle $-\beta_i$. It is clear that the x_i axis in frame $\mathbf{I}_i$ coincides with $\boldsymbol{u}_i$; i.e., $\boldsymbol{u}_{i,\mathrm{I}_i} = [1,0,0]^T$. Following the rotation rules of coordinate systems in $\mathbb{R}^3$ (see, e.g., [16]), it is easy to show that for any vector $\boldsymbol{v}$, $\boldsymbol{v}_{\mathrm{I}_i} = R_i \cdot \boldsymbol{v}$ or $\boldsymbol{v} = R_i^T \cdot \boldsymbol{v}_{\mathrm{I}_i}$, where R_i is the rotation matrix from frame $\mathbf{A}$ to frame $\mathbf{I}_i$ whose expression is given as $R_i = R_{\boldsymbol{y}}(-\beta_i) R_{\boldsymbol{z}}(\alpha_i)$, where

$$R_{\boldsymbol{z}}(\alpha_i) = \begin{bmatrix} \cos\alpha_i & \sin\alpha_i & 0 \\ -\sin\alpha_i & \cos\alpha_i & 0 \\ 0 & 0 & 1 \end{bmatrix}$$

and

$$R_{\boldsymbol{y}}(-\beta_i) = \begin{bmatrix} \cos\beta_i & 0 & \sin\beta_i \\ 0 & 1 & 0 \\ -\sin\beta_i & 0 & \cos\beta_i \end{bmatrix}.$$

B. Poisson Measurement Model

From the nature of the particle-counting process, we assume the following Poisson probability mass function (PMF) model for each detector's particle count:

$$\mathrm{P}\{y_{i,j}(t) = y\} = \frac{e^{-\lambda_{i,j}t}(\lambda_{i,j}t)^y}{y!}, \quad y = 0, 1, 2, \ldots, \tag{1}$$

where $y_{i,j}(t)$ is the stochastic measurement of the jth detector in the ith eyelet (or the i,jth detector; $i = 1, \ldots, M$, $j = 1, \ldots, N$) within time window $[0, t]$, and $\lambda_{i,j}$ is the particle counting rate of that detector. Obviously, the determination of $\lambda_{i,j}$ is the foremost issue in the practical modeling, since it statistically characterizes the detector's measurement.

From a signal processing viewpoint, the detection rate $\lambda_{i,j}$ of the i,jth detector can be naturally expressed as

$$\lambda_{i,j} = \lambda_{i,j,\mathrm{s}} + \lambda_{i,j,\mathrm{n}} \tag{2}$$

where $\lambda_{i,j,\mathrm{s}}$ and $\lambda_{i,j,\mathrm{n}}$ are, respectively, the expected particle counting rate of the i,jth detector coming from the source(s) and the noise. We consider two categories of noise: the count of particles coming from noise sources outside the array and the erroneous particle counts due to inner measurement (e.g., electronic or thermal) errors. From the remote and time-invariant point-source assumptions, we assume the source-particle intensity coming from different directions $\boldsymbol{u}$ is homogeneous over the array's surface and time invariant; similarly, the noise intensity is also assumed[5] to be isotropic, homogenous, and time invariant throughout the array.

As a specific model based on Section III and (2), we consider the simplest rank-1 PG basis function model of $\lambda_{i,j}$

$$\lambda_{i,j} = \Omega_{i,j} a_{i,\mathrm{CS}} \left[\mu \mathcal{N}(\boldsymbol{u}; \boldsymbol{u}_{i,j}, \sigma^2 I) + \eta\right] \tag{3}$$

where $\Omega_{i,j}$ is the solid angle of the cone of associated directions of the i,jth detector, $a_{i,\mathrm{CS}}$ is the ith eyelet's detection cross section area with respect to $\boldsymbol{u}$, μ is the exciting source particles intensity at the array surface (in $\mathrm{s}^{-1}\mathrm{m}^{-2}$) ignoring the sensor's presence, η is the angular density of the noise particles intensity at the array surface[6] (in $\mathrm{s}^{-1}\mathrm{m}^{-2}\mathrm{rad}^{-2}$), and $\mathcal{N}(\boldsymbol{u}; \boldsymbol{u}_{i,j}, \sigma^2 I)$ denotes the circular Gaussian LSF:

$$\begin{aligned} \mathcal{N}(\boldsymbol{u}; \boldsymbol{u}_{i,j}, \sigma^2 I) &\triangleq \frac{1}{2\pi\sigma^2} e^{-\frac{1}{2\sigma^2}(\boldsymbol{u}-\boldsymbol{u}_{i,j})^T(\boldsymbol{u}-\boldsymbol{u}_{i,j})} \\ &= \frac{1}{2\pi\sigma^2} e^{\left(\boldsymbol{u}_{i,j}^T \boldsymbol{u} - 1\right)/\sigma^2}. \end{aligned} \tag{4}$$

In (4), $\boldsymbol{u}_{i,j}$ is the associated source direction of the i,jth detector and σ is the angular standard deviation of the Gaussian LSF (in radians), which depends on the lens surface shape and optical properties. Comparing (2) and (3), we have $\lambda_{i,j,\mathrm{s}} = \Omega_{i,j}\mu a_{i,\mathrm{CS}} \mathcal{N}(\boldsymbol{u}; \boldsymbol{u}_{i,j}, \sigma^2 I)$ and $\lambda_{i,j,\mathrm{n}} = \Omega_{i,j} a_{i,\mathrm{CS}} \eta$, indicating a good match between the mathematical and practical interpretations of $\lambda_{i,j}$. The vector of unknown parameters is then $\boldsymbol{\theta} = [\phi, \psi, \mu, \eta]^T$.

In Sections V and VI, we will discuss how to calculate the parameters and variables defined above on a practical basis, how they are associated with physical configurations of the array, and what their fundamental limitations are.

Remark 4.1: Gaussian-shaped point-spread functions (PSFs) for lens systems are widely used in the optical discipline. Examples include optical lenses [17], scanning laser ophthalmoscopes [18], stellar photometry [19], and plasma lenses [20]. Moreover, Gaussian functions are commonly used to describe the angular sensitivity function (ASF) of a retina cell in the compound-eye literature (see, e.g., [21]).

[5]This assumption is made only for simplicity.

[6]We assume $\eta = \eta_{\mathrm{out}} + \eta_{\mathrm{in}}$, where η_{out} and η_{in} correspond to the noise coming from outside the array (e.g., noisy particle-emitting sources) and those inside the array (e.g., thermal or electronic noises), respectively.

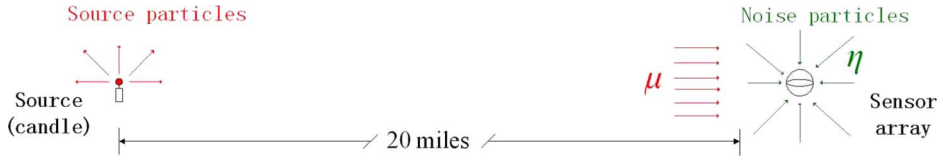

Fig. 4. Candle and the detector array.

TABLE III
LIST OF VARIABLES USED IN NUMERICAL EXAMPLES

Variables	Unit	Definition & Description
M	–	number of eyelets in the array
N	–	number of detectors in each eyelet (or sub-array)
ϕ , ψ	rad	azimuth and elevation angles of the source direction (in the array's reference frame)
μ	$\mathrm{s}^{-1}\mathrm{m}^{-2}$	exciting source particle intensity at the array surface
η_{out}, η_{in}	$\mathrm{s}^{-1}\mathrm{m}^{-2}\mathrm{rad}^{-2}$	angular density of noise particle intensity at the array surface due to outside and inside noise sources, respectively
η	$\mathrm{s}^{-1}\mathrm{m}^{-2}\mathrm{rad}^{-2}$	total angular density of noise particle intensity at the array surface, $\eta = \eta_{\mathrm{out}} + \eta_{\mathrm{in}}$
LSNR	–	local signal-to-noise ratio, defined as $\mu/(2\pi\sigma^2\eta)$
SNR_i	–	ith eyelet's signal-to-noise ratio (we use $10\log_{10}(\mathrm{SNR}_i)$ with unit dB in examples)
σ	rad	angular standard deviation of the circular Gaussian lens-shaping function
k_{a}	–	angular expansion factor of the eyelet
R	m	radius of the spherical array
R_{d}	m	distances from the array center to the edge of a sub-array
h_{d}	m	distance from a lens center to the center of the corresponding sub-array DS
l_{d}	m	distances from the array center to the center of the sub-array DS
r_{l}, r_{s}, r_{d}	m	radius of the circular lens, sub-array, and (perhaps non-circular) detector, respectively
σ_x	m	standard deviation of the Gaussian particle intensity distribution on the sub-array DS, $\sigma_x \simeq \sigma R_{\mathrm{d}}/k_{\mathrm{a}}$ for small σ
pe_{l}	–	packing efficiency of the circular lenses on the surface of the spherical array
pe_{d}	–	packing efficiency of the hexagonal detectors on the circular sub-array DS, $\mathrm{pe}_{\mathrm{d}} = 1$
ESC	–	the expected count of source particles during the observation time window t

Remark 4.2: Model (3) has the property that all its parameters can be experimentally calibrated (i.e., externally observable). Hence, we may consider it as a "minimal model."

Remark 4.3: The i,jth detector's associated source direction $\boldsymbol{u}_{i,j}$ is defined as the unit vector direction of the point-like source that maximizes the detector's particle counting rate. In other words, source particles coming from $\boldsymbol{u}_{i,j}$ should focus on the detection surface of the i,jth detector. The method used to determine $\boldsymbol{u}_{i,j}$ is given in Section V.

Remark 4.4: Note that $\mathcal{N}(\boldsymbol{u};\boldsymbol{u}_{i,j},\sigma^2 I) = \mathcal{N}(\boldsymbol{u}_{i,j};\boldsymbol{u},\sigma^2 I)$. In other words, while the Gaussian LSF describes a distribution of detection rate with respect to $\boldsymbol{u}$ centered at $\boldsymbol{u}_{i,j}$, equivalently, it also defines a "focusing distribution" of $\boldsymbol{u}_{i,j}$ centered at $\boldsymbol{u}$: detectors with associated directions closer to source direction $\boldsymbol{u}$ have higher detection rates; and σ describes the width of the Gaussian LSF. In addition, the circular Gaussian LSF (4) is simple, in the sense that it is linear in $\boldsymbol{u}$ in the exponent and invariant to the chosen reference frame.

V. A PROTOTYPE MODEL AND ITS PARAMETERS μ AND η_{out}

As discussed, model (3) is particularly applicable for the proposed compound-eye array. Its parameters, such as μ and η, are determined according to practical applications. As a practical example (which will be used as the numerical example in the second part of the paper), we consider the problem of localizing a candle from 20 miles away on a clear night, assuming no moonlight but regular starlight, as shown in Fig. 4. This is the weakest light source that a normal naked human eye can detect [22]. We treat both the signal source (the candle) and the noise sources (the stars) according to the theory of black-body radiation [23]. In Appendix A, we estimate the *attenuated* values of parameters μ and η_{out} in this environment as

$$\mu \approx 4.766 \times 10^7 \ \mathrm{s}^{-1}\mathrm{m}^{-2}$$

and

$$\eta_{\mathrm{out}} \approx 1.9 \times 10^{10} \ \mathrm{s}^{-1}\mathrm{m}^{-2}\mathrm{rad}^{-2}.$$

VI. HARDWARE SETUP AND FUNDAMENTAL LIMITATIONS OF THE ARRAY

In this section, we discuss the hardware setup of the array by defining its essential configurational variables. We also consider the fundamental limitations of these variables, which will constrain the configuration of any real-world implementation of such an array.

A. Hardware Setup

In Table III, we list the configuration variables of the hardware setup of the array, which are also shown schematically in Fig. 5. In the following, we associate the directions $\boldsymbol{u}_{i,j}$ in model (4), with the array's physical variables.

We determine the associated source direction of the i,jth detector in the ith eyelet's reference frame $\mathbf{I}_i$, with all involved variables shown in Fig. 5. Define the *radial direction* of the i,jth detector as a unit vector $\boldsymbol{v}_{i,j}$ along the line joining the

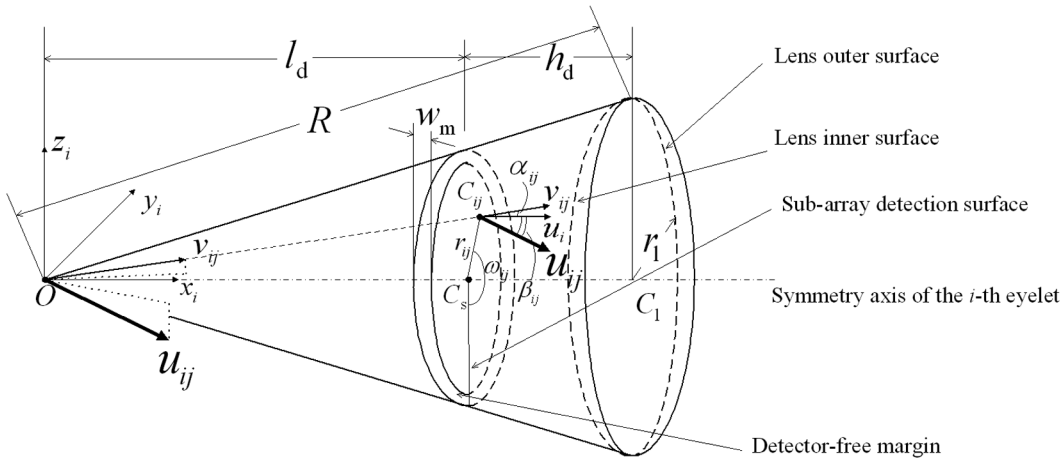

Fig. 5. Determination of $\boldsymbol{u}_{i,j}$ in the ith eyelet's reference frame.

spherical array center O and the center of the i,jth detector $C_{i,j}$ and pointing outward from the spherical array; and $\boldsymbol{u}_i$ as a unit vector in the (outward) direction of the symmetry axis of the ith eyelet. Let points $C_{\rm s}$ and C_1 be the center of the subarray DS and the center of mass of the lens, respectively. Define $\alpha_{i,j}$ as the angle between $\boldsymbol{v}_{i,j}$ and $\boldsymbol{u}_i$, and define $\beta_{i,j}$ as the angle between $\boldsymbol{u}_{i,j}$ and $\boldsymbol{u}_i$.

Because of the focusing effect of the lens, the associated direction $\boldsymbol{u}_{i,j}$ generally differs from the radial direction $\boldsymbol{v}_{i,j}$ of the i,jth detector (if $C_{i,j} \neq C_{\rm s}$). By Snell's law (see, e.g., [24]), we have i) $\alpha_{i,j} < \beta_{i,j}$[7]; ii) $\boldsymbol{v}_{i,j}$ and $\boldsymbol{u}_{i,j}$ lie on both side of $\boldsymbol{u}_i$; and iii) $\boldsymbol{v}_{i,j}$, $\boldsymbol{u}_{i,j}$, and $\boldsymbol{u}_i$ are on the same plane. We then define the *angular expansion factor* of the i,jth detector as $k_{{\rm a},i,j} = \beta_{i,j}/\alpha_{i,j}$. Note that in general $k_{{\rm a},i,j}$ may be different for different i and j, but when the conical module of each eyelet is narrow (i.e., $r_1 \ll R$) we assume it to be a constant for all i and j, denoted by $k_{\rm a}$. Similar to σ, $k_{\rm a}$ completely depends on the lens properties: shape of inner and outer surfaces, refractive factors, etc.

By the definition of $k_{{\rm a},i,j}$ and the above observations ii) and iii), we can determine $\boldsymbol{u}_{i,j}$ in frame $\mathbf{I}_i$ by

$$\boldsymbol{u}_{i,j,{\rm I}} = \frac{\boldsymbol{s}}{\|\boldsymbol{s}\|} \tag{5}$$

where $\boldsymbol{s} = [r_{i,j}/\tan(k_{{\rm a},i,j}\tan^{-1}(r_{i,j}/l_{\rm D})), -r_{i,j}\cos\omega_{i,j}, -r_{i,j}\sin\omega_{i,j}]^T$. Then $\boldsymbol{u}_{i,j} = R_i^T\boldsymbol{u}_{i,j,{\rm I}}$.

B. Limitations of Array Variables

We discuss in Theorem 6.1 the fundamental limitations on several of the array variables as defined above.

Theorem 6.1: The following fundamental limitations with minimal particle wavelength $\lambda_{\min}$ apply to array variables $k_{\rm a}$, σ_x, and σ:

$$k_{\rm a} \geq \frac{2}{\sqrt{3}}, \quad (M \gg 1) \tag{6a}$$

$$\sigma_x \geq \sigma_{x,{\rm B}} = \frac{\lambda_{\min}}{2\sqrt{2}\pi\sqrt{1-(h_{\rm d}/r_1)^2\ln\left[1+(r_1/h_{\rm d})^2\right]}}, \tag{6b}$$

$$\sigma \geq \max\left\{\frac{k_{\rm a}\sigma_{x,{\rm B}}}{R_{\rm d}}, \frac{x_{0,1}\lambda_{\min}}{2\sqrt{2}\pi r_1}\right\}, \tag{6c}$$

where $x_{0,1}$ is the first positive zero of the Bessel function J_0.

Proof: See Appendix B.

VII. Performance Measure and Its Fundamental Bounds

For analyzing the array's performance in localizing particle sources, a natural candidate for the performance measure could be the Cramér–Rao bound (CRB) matrix of the unknown parameter vector $\boldsymbol{\theta}$. However, a meaningful scalar quantity is more appropriate than a matrix measure since scalar quantities are easier to compare. In [25], we defined the mean-square angular error (MSAE) of any source direction estimator as $\mathrm{MSAE}_{\rm estimator} \triangleq \mathrm{E}(\delta^2)$, where δ is the angular error between $\boldsymbol{u}$ and its estimate $\hat{\boldsymbol{u}}$. Clearly, $\mathrm{MSAE}_{\rm estimator}$ depends on the array configuration, the estimation algorithm, the value of unknown parameters $\boldsymbol{\theta}$, and the length of observation time window t. Another (DOA independent) performance measure $\mathrm{MSAE}_{\rm av}$ is the (uniform) average of $\mathrm{MSAE}(\boldsymbol{u})$ over the US.

Moreover, we defined in [25] (see also [26]) another quantity:

$$\mathrm{MSAE}_{\rm CRB} \triangleq \cos^2\psi\cdot\mathrm{CRB}(\phi) + \mathrm{CRB}(\psi) \tag{7}$$

where $\mathrm{CRB}(\phi)$ and $\mathrm{CRB}(\psi)$ are the (scalar) Cramér–Rao bounds for the azimuth and elevation angles, respectively. We showed that for any regular model and estimator, $\lim_{K\to\infty} K\cdot\mathrm{MSAE}_{\rm estimator} \geq K\cdot\mathrm{MSAE}_{\rm CRB}$, where K is the number of snapshots, which is proportional to t and R^2 in this case. Thus, $\mathrm{MSAE}_{\rm CRB}$ serves as an asymptotic lower bound on $\mathrm{MSAE}_{\rm estimator}$.

It follows that $\mathrm{MSAE}_{\rm CRB}$ is i) independent of the estimation algorithm, ii) an asymptotically tight bound attainable by some second-order efficient regular estimators (usually the maximum-likelihood estimator (MLE); see, e.g., [27]), and iii) invariant to the choice of reference coordinate frame, since the information content in the data is invariant under rotation. Considering the above desirable properties, we use $\mathrm{MSAE}_{\rm CRB}$ as a performance measure showing the best asymptotic accuracy for each specific array in source-direction estimation. We will

[7]This is valid since the lens refractive index is always larger than that of the array's environment.

derive the $\mathrm{MSAE}_{\mathrm{CRB}}$ for the proposed array in the second part of this paper [28].

A. *Universal Bound 1:* $\mathrm{MSAE}_{\mathrm{UB}}$

Now that we know that $\mathrm{MSAE}_{\mathrm{CRB}}$ indicates the optimal performance of a specific array configuration, we can now ask the following question: What is the "best" performance of an *arbitrary* array in principle? We try to answer this question by proposing a *universal* lower bound on MSAE, denoted by $\mathrm{MSAE}_{\mathrm{UB}}$, for an arbitrary array inside a sphere with radius R, regardless of the array's hardware or software configuration; i.e., $\mathrm{MSAE}_{\mathrm{UB}} \leq \mathrm{MSAE}$, $\forall$ array configurations. For this universal lower bound, we assume that neither outside noise (from noise particle sources) nor inside electronic/thermal noise is present. We need also the following (reasonable) assumption.

Assumption 7.1: "Practical" assumption: It is impossible to estimate by any combination of hardware and software the DOA of incoming particles during a certain time window better then the inherent MSAE of the (stochastic) direction of their total momentum. (Note that their total momentum is stochastic because of the quantum-mechanical uncertainty principle.)

The following theorem follows from derivations based on the uncertainty principle of quantum mechanics (see, e.g., [29] and [30]).

Theorem 7.1: Under Assumption 7.1, a universal lower bound on the MSAE (respectively, $\mathrm{MSAE}_{\mathrm{av}}$) of any direction-of-arrival (DOA) estimator based on measurements from *any* sensing hardware contained inside a sphere with radius R is

$$\mathrm{MSAE}_{\mathrm{UB}} = \frac{1}{\mathrm{ESC}} \left(\frac{x_{0,1} \cdot \lambda_{\min}}{2\pi R} \right)^2$$

whenever

$$\mathrm{MSAE}_{\mathrm{UB}} \leq \frac{\mathrm{MSAE}_0(\boldsymbol{u})}{2 - e^{-\mathrm{ESC}}} \tag{8}$$

(respectively, whenever $\mathrm{MSAE}_{\mathrm{UB}} \leq \mathrm{MSAE}_0/(2 - e^{-\mathrm{ESC}})$), where $x_{0,1} \simeq 2.405$ is the first positive zero of the Bessel function of order 0, $\lambda_{\min}$ is the minimal wavelength of the incident particles, $\mathrm{MSAE}_0(\boldsymbol{u})$ is $\mathrm{MSAE}(\boldsymbol{u})$ without detected source particles, and $\mathrm{MSAE}_0 = \pi^2/2 - 2$ is the $\mathrm{MSAE}_{\mathrm{av}}$ without detected source particles—which is uniformly attained by the MSAE of a random estimator with uniform distribution over the US.

Proof: See Appendix C.

Remark 7.1: The derivation of $\mathrm{MSAE}_{\mathrm{UB}}$ may be improved for wideband energy/wavelength particles. (The partition of the wavelength bandwidth into several narrow bands should lead to the replacement of $\lambda_{\min}$ in (8) by the inverse of the rms value of $1/\lambda$.)

B. *Universal Bound 2:* $\mathrm{MSAE}_{\mathrm{UCR}}$

Another important universal bound for any DOA estimator for the source direction $\boldsymbol{u}$ can be found using an interesting method similar to the $\mathrm{MSAE}_{\mathrm{UB}}$ derivation. This bound is obtained via the usual CRB expression; but instead of being dependent on the measurement model of any specific sensor, it depends on the wave function $\hat{\psi}(E, \boldsymbol{p})$ for the energy-momentum density distribution. Note that this is not the usual $\psi(x,t)$ for space–time density distribution, which can be seen by exploiting the fact that $\hat{\psi}$ is proportional to the Fourier transform (or characteristic function) of the usual ψ. Then, minimization of the CRB over possible $\hat{\psi}$ functions (i.e., possible sensors hardware) is equivalent to a maximization problem with respect to ψ. This gives a truly universal lower bound for the $\mathrm{MSAE}_{\mathrm{CRB}}$ of any possible hardware. This bound, which may be denoted as universal CRB or $\mathrm{MSAE}_{\mathrm{UCR}}$, is both looser and simpler than $\mathrm{MSAE}_{\mathrm{UB}}$.

The need for the UCR stems from the fact that the $\mathrm{MSAE}_{\mathrm{UB}}$ is in fact a lower bound for the MSAE of the stochastic direction of the total momentum of the source particles with respect to $\boldsymbol{u}$; i.e., if the direction of the total momentum may be regarded as "DOA estimator"—even though it cannot be observed directly, its MSAE with respect to $\boldsymbol{u}$ can still be used as a lower bound for any estimator of it. The problem with $\mathrm{MSAE}_{\mathrm{UB}}$ is that we try to find a universal lower bound not for the MSAE of estimators for the total momentum direction, but instead for MSAE of estimators of the source direction $\boldsymbol{u}$. Thus, another approach for such a universal bound is needed.

Theorem 7.2: A universal lower bound on the $\mathrm{MSAE}_{\mathrm{CRB}}$ for *any DOA* estimator based on measurements from *any* sensing hardware contained inside a sphere with radius R is

$\mathrm{MSAE}_{\mathrm{UCR}} \cdot (1 - e^{-\mathrm{ESC}})^2$, where

$$\mathrm{MSAE}_{\mathrm{UCR}} \triangleq \frac{1}{\mathrm{ESC}} \left(\frac{\lambda_{\min}}{2\pi R} \right)^2. \tag{9}$$

Proof: See Appendix C.

Remark 7.2: Note that Remark 7.1 applies also to (9), and

$$\sqrt{\frac{\mathrm{MSAE}_{\mathrm{UCR}}}{\mathrm{MSAE}_{\mathrm{UB}}}} = \frac{1}{x_{0,1}} \approx \frac{1}{2.405}.$$

VIII. Conclusion

In this part, we proposed a novel particle-detector array inspired by the biological compound eye and statistically modeled its behavior. This array combines the advantages of biological compound eyes (e.g., large field of view) and human eyes (e.g., high spatial resolution). It can be used to localize optical, radioactive, or cosmic sources from the far field. To analyze the array's performance, we presented a mathematical minimal model for the array's measurements and gave an example to illustrate how the parameters in the model can be determined in practice. We then defined the array's physical variables and associated them with the proposed mathematical model. In addition, we discussed the performance measure of the array and derived its fundamental bounds. Part I forms the analytical basis for the second part of this paper, in which we will use the proposed measurement model to analyze the performance of the array, both analytically and numerically.

We believe that the proposed array potentially has a wide impact on optics, security, and astronomy assisted applications. The fact that an artificial compound eye with similar structure and function to its biological counterpart was recently built makes this closer into reality.

A. Future Work

In future work, the current model can be extended by considering the correlation effects among incident particles (e.g., multipath scattering and polarization effects) by introducing a *complex* transfer function, time-variant particle intensity (which is essential for particle communication), particles with wide energy spectrum (to extract more source parameters, e.g., temperature), adaptive optics, multifocal lenses and polarization filters. Other extensions may include eyelet and lens-shape optimization, adaptive estimation of the directions of multiple sources, and investigation of the channel capacity for particle communication using the array.

APPENDIX A
ESTIMATION OF μ AND η_{out} IN SECTION V

A. Estimation of μ

Assume that the array detects only visible photons, i.e., the electromagnetic radiation within wavelength range $[\lambda_1, \lambda_2]$, where $\lambda_1 = 0.4 \times 10^{-6}$ m and $\lambda_2 = 0.7 \times 10^{-6}$ m. We recall Planck's law of black-body radiation [23]: $P_\lambda = 2\pi hc^2/\lambda^5(e^{hc/\lambda kt} - 1)$, where P_λ is the power of radiation per source surface area per wavelength (in Jm^{-3}), h is Planck's constant (6.626×10^{-34} Js), c is the speed of light in a vacuum (3×10^8 ms^{-1}), λ is the wavelength of a photon (in m), k is the Boltzmann constant (1.38×10^{-23} JK^{-1}), and T is the temperature on the source surface (in K). Also note that the energy of a single photon is $E_\lambda = hc/\lambda$; thus the number per second of photons emitted per source surface area)m^2) per wavelength (m) is computed as $C_\lambda = P_\lambda/E_\lambda$. The unit of P_λ is $\text{Js}^{-1}\text{m}^{-3}$ and that of C_λ is $\text{s}^{-1}\text{m}^{-3}$.

For simplicity, we also assume a candle flame to be roughly spherical with radius $r_c = 1$ cm and the intensity of its radiation to be isotropic. The surface temperature of the flame is roughly 1800 K [31]. Neglecting (temporarily) the atmospheric photon absorption and assuming isotropic medium, it follows that the source photon intensity per unit wavelength at a distance r from the source, is given by $I(\lambda; r, T) = (r_c^2/r^2)(2\pi c/\lambda^4(e^{hc/(\lambda kT)} - 1))$. Hence, $\mu = \int_{\lambda_1}^{\lambda_2} I(\lambda; r, T)\text{d}\lambda$.

Using the notation $\lambda_0 = hc/kT$, the substitution $x = \lambda_0/\lambda$ gives $\mu = 2\pi c\lambda_0^{-3}(r_c^2/r^2)\int_{x_2}^{x_1}(x^2/(e^x - 1))\text{d}x$, where $x_1 = \lambda_0/\lambda_1$ and $x_2 = \lambda_0/\lambda_2$. The last integral can be evaluated as $\phi(x_2) - \phi(x_1)$, using the function $\phi(x) \triangleq \int_x^\infty (t^2/(e^t - 1))\text{d}t = \sum_{k=1}^\infty [e^{-kx}((x^2/k) + (2x/k^2) + (2/k^3))]$, $x > 0$, where the expansion for $\phi(x)$ follows by termwise integration of the integrand expansion (into powers of e^{-t}). It can be shown that for the truncated expansion, the error term is bounded by the first neglected term times $(1 - e^{-x})^{-1}$.

Using the above values, we get $\lambda_0 = 8 \times 10^{-6}$ m, $x_1 = 20$, and $x_2 = 11.43$. The computation gives (using only the first term of the expansion) $\phi(x_2) - \phi(x_1) \approx 1.6886 \times 10^{-3}$, hence (for $r = 20$ miles)

$$\mu = 6.003 \times 10^8 \approx 6 \times 10^8 \text{ s}^{-1}\text{m}^{-2}.$$

This is the *unattenuated* value of μ.

Remark A.1: In order to evaluate the attenuated value of μ due to atmospheric absorption, we assume the attenuation factor (due e.g., to fog condition) to be 1.1 db/mile—resulting (for $r = 20$ miles) by a total 22 db (or 12.589) for the attenuation factor, hence the *attenuated (practical)* value for μ is

$$\mu = \frac{6 \times 10^8}{12.589} \approx 4.766 \times 10^7 \text{ s}^{-1}\text{m}^{-2}. \tag{A.1}$$

B. Estimation of η_{out}

We can write $\eta_{\text{out}} = \eta_{\text{a}} + \eta_{\text{G}} + \eta_{\text{U}}$, where η_{a} represents the contribution from the air surrounding the sensor, η_{G} represents the contribution from our galaxy (milky way), and η_{U} represents the contribution from all the other galaxies in the universe.

Computation of η_{a}: In this case, denote the source (surrounding air) temperature by T_{a}. Then η_{a} is given by the photon intensity (due to surrounding air molecules) into the sensor surface divided by $2\pi\text{rad}^2$, since these photons are arriving to each point on the sensor surface from only one hemisphere of directions corresponding to this point. Hence, η_{a} per unit wavelength is given by $\eta_{\text{a}}(\lambda) = (1/2\pi)I(\lambda; r_c, T_{\text{a}}) = c\lambda^{-4}/(e^{hc/(\lambda kT_{\text{a}})} - 1)$. Therefore, $\eta_{\text{a}} = \int_{\lambda_1}^{\lambda_2} \eta_{\text{a}}(\lambda)\text{d}\lambda$. Using the notation $\lambda_0 = hc/kT_{\text{a}}$, and the substitutions $x = \lambda_0/\lambda$, $x_1 = \lambda_0/\lambda_1$, $x_2 = \lambda_0/\lambda_2$. We get $\eta_{\text{a}} = c\lambda_0^{-3}[\phi(x_2) - \phi(x_1)]$. Assuming $T_{\text{a}} = 280$ deg K, we have $\lambda_0 = 5.144 \times 10^{-5}$ m, $x_1 = 128.6$, $x_2 = 73.49$, $\phi(x_2) - \phi(x_1) \approx 6.73 \times 10^{-29}$. Hence, $\eta_{\text{a}} \approx 1.483 \times 10^{-7}$ $\text{s}^{-1}\text{m}^{-2}\text{rad}^{-2}$.

Computation of η_{G}: In this case, we have to estimate the contribution of our galaxy's stars (except the sun!) to η_{out}. Since our solar system is located inside a spiral arm of our galaxy (milky way) whose local width in the neighborhood of our solar system is estimated by 200 pc (parsec) which is about 650 ly (light year), we approximate our galaxy contribution to η_{out} by a spherical cluster of stars with radius $R_{\text{G}} = 300$ ly (about half the local width of the spiral arm), centered at our solar system. In this case we can treat the stars in this cluster as stationary (hence ignoring relativistic effects due to Hubble cosmological expansion low).

The photon intensity per unit wavelength arriving to the sensor from a star at distance r with radius R_{S} and surface temperature T_{S} is given by $I(\lambda; r) = (R_{\text{S}}/r)^2(2\pi c\lambda^{-4}/(e^{\lambda_0/\lambda} - 1))$, where $\lambda_0 \triangleq hc/kT_{\text{S}}$. Integration over λ gives the photon intensity at the sensor due to a star at distance r as $\mu(r) = \int_{\lambda_1}^{\lambda_2} I(\lambda; r)\text{d}\lambda$. The substitutions $x = \lambda_0/\lambda$, $x_1 = \lambda_0/\lambda_1$, $x_2 = \lambda_0/\lambda_2$ gives $\mu(r) = 2\pi c\lambda_0^{-3}(R_{\text{S}}/r)^2[\phi(x_2) - \phi(x_1)]$. The photon flux arriving from the star to the sensor is given by $\pi R^2\mu(r)$ where R denotes the sensor radius. Thus, the photon flux due to stars inside a spherical shell with radius r and width $\text{d}r$ is $\pi R^2\mu(r)\text{d}N(r) = \pi R^2\mu(r)4\pi\rho_{\text{G}}r^2\text{d}r$, where $N(r) = (4\pi/3)\rho_{\text{G}}r^3$ denotes the number of stars inside a spherical shell of radius r and average density of ρ_{G} stars per unit volume. Consequently, the photon flux arriving to the sensor from the spherical cluster (with radius R_{G}) of stars should be $\int_0^{R_{\text{G}}} \pi R^2\mu(r)\text{d}N(r)$.

The resulting photon intensity at the sensor due to the star cluster is $\mu_{\text{G}} = 1/(4\pi R^2)\int_0^{R_{\text{G}}} \pi R^2\mu(r)\text{d}N(r) = (1/4)\int_0^{R_{\text{G}}} \mu(r)\text{d}N(r)$. Since for each point on the sensor,

incoming photons are arriving from only one hemisphere of directions, it follows that the resulting $\eta_{\rm G}$ is found from $\mu_{\rm G}$ by dividing it by $2\pi{\rm rad}^2$; hence $\eta_{\rm G} = \mu_{\rm G}/(2\pi)$. Using the above expressions for $\mu(r)$ and $N(r)$, we get $\eta_{\rm G} = \pi c\lambda_0^{-3}\rho_{\rm G}R_{\rm S}^2R_{\rm G}[\phi(x_2) - \phi(x_1)]$. To estimate $\rho_{\rm G}$, we estimate the average number of stars per unit volume inside a sphere of radius 50 ly centered at our sun. It is known [32] that the number of such stars is about 1000; therefore, $\rho_{\rm G} \approx 1000/(4\pi/3 \times (50\,{\rm ly})^3) \approx 2.256 \times 10^{-51}\ {\rm m}^{-3}$.

Since our sun can be considered as an "average star," we estimate the star radius $R_{\rm S}$ and its surface temperature $T_{\rm S}$ by these parameters of our sun; i.e., we choose $R_{\rm S} = 7 \times 10^8$ m, $T_{\rm S} = 6000$ deg K, and get $\lambda_0 = 2.4 \times 10^{-6}$ m, $x_1 = 6$, $x_2 \approx 3.43$, $\phi(x_2) - \phi(x_1) \approx 0.5523$. Hence, $\eta_{\rm G} \approx 1.18 \times 10^{11}\ {\rm s}^{-1}{\rm m}^{-2}{\rm rad}^{-2}$.

Computation of $\eta_{\rm U}$: In this case, we have to estimate the contribution of the other galaxies to η. As we shall see, relativistic Doppler effect (due to relativistic cosmological expansion) should be taken into account. Denote by $N_{\rm U}$ the number of stars in the other galaxies (which is almost their number in the universe!) and by $R_{\rm U}$ the universe radius. For simplicity, we use the simplest cosmological expansion model (Hubble law) according to which the average receding velocity of a star at distance r from an observer is given by $v = c(r/R_{\rm U})$. Therefore, sufficiently far galaxies should have relativistic velocities which should be taken into account. We denote by $\lambda_{\rm S}$ the wavelength of a photon emitted from a star in the *star frame*, and by $\lambda_{\rm D}$ the wavelength of this photon as observed in the *detector frame*. It follows from (relativistic) Doppler effect that $\lambda_{\rm S}/\lambda_{\rm D} = \sqrt{(1-v/c)/(1+v/c)}$. Hence, by Hubble law $\lambda_{\rm S}/\lambda_{\rm D} = \sqrt{(1-r/R_{\rm U})/(1+r/R_{\rm U})}$. Let $T_{\rm S} = \lambda_{\rm S}/c$ be the photon time period in the star frame, and $T_{\rm D} = \lambda_{\rm D}/c$ denote the photon time period in the detector frame. Standard (even nonrelativistic) physical consideration shows that the number of incoming photons with bandwidth ${\rm d}\lambda_{\rm S}$ to the detector during period $T_{\rm S}(1 - v/c)$ in the star frame is identical to the corresponding number of incoming photons with bandwidth ${\rm d}\lambda_{\rm D}$ to the detector during period $T_{\rm D}$ in the detector frame. This equality can be written as $I_{\rm D}(\lambda_{\rm D};r){\rm d}\lambda_{\rm D}T_{\rm D} = I_{\rm S}(\lambda_{\rm S};r){\rm d}\lambda_{\rm S}T_{\rm S}(1 - v/c)$, where $I_{\rm S}(\lambda_{\rm S};r)$ is the photon intensity per wavelength $\lambda_{\rm S}$ at distance r in the *star* frame, while $I_{\rm D}(\lambda_{\rm D};r)$ is the corresponding photon intensity as observed in the *detector* frame. Therefore, $I_{\rm D}(\lambda_{\rm D};r) = I_{\rm S}(\lambda_{\rm S};r)({\rm d}\lambda_{\rm S}/{\rm d}\lambda_{\rm D})T_{\rm S}/T_{\rm D}(1 - v/c)$. Since $T_{\rm S}/T_{\rm D} = \lambda_{\rm S}/\lambda_{\rm D} = {\rm d}\lambda_{\rm S}/{\rm d}\lambda_{\rm D} = \sqrt{(1-v/c)/(1+v/c)}$, we get $I_{\rm D}(\lambda_{\rm D};r) = I_{\rm S}(\lambda_{\rm S};r)(1-v/c)^2/(1+v/c) = I_{\rm S}(\lambda_{\rm S};r)(1-r/R_{\rm U})^2/(1 + r/R_{\rm U})$. In the star system $I_{\rm S}(\lambda_{\rm S};r) = (R_{\rm S}/r)^2 2\pi c\lambda_{\rm S}^{-4}[e^{\lambda_0/\lambda_{\rm S}} - 1]^{-1}$, where $\lambda_0 \triangleq hc/(kT_{\rm S})$. Since $\lambda_{\rm D}/\lambda_{\rm S} = \sqrt{(1+r/R_{\rm U})/(1-r/R_{\rm U})}$, we have $I_{\rm S}(\lambda_{\rm S};r) = (R_{\rm S}/r)^2 2\pi c\lambda_{\rm D}^{-4}[(1+r/R_{\rm U})/(1-r/R_{\rm U})]^2[e^{\lambda_0/\lambda_{\rm S}} - 1]^{-1}$.

Hence, $I_{\rm D}(\lambda_{\rm D};r) = I_{\rm S}(\lambda_{\rm S};r)(1 - r/R_{\rm U})^2/(1 + r/R_{\rm U}) = (R_{\rm S}/r)^2 2\pi c\lambda_{\rm D}^{-4}(1+r/R_{\rm U})/(e^{(\lambda_0/\lambda_{\rm D})\sqrt{(1+r/R_{\rm U})/(1-r/R_{\rm U})}} - 1)$. This is the desired relativistic intensity expression in the *detector* frame.

Denote by $\rho_{\rm U}$ the average number of stars per unit volume in the universe. Clearly, $\rho_{\rm U} = N_{\rm U}/(4\pi/3R_{\rm U}^3)$ where $N_{\rm U}$ denotes the number of stars in the universe and $R_{\rm U}$ denotes the universe radius. Since there are about 10^{11} galaxies in the universe and the number of stars in an average galaxy is estimated by 10^{11}, we estimate $N_{\rm U} \approx 10^{22}$, while the current estimate for $R_{\rm U}$ is 1.3×10^{10} ly, which gives $\rho_{\rm U} \approx 1.2829 \times 10^{-57}\ {\rm m}^{-3}$.

The photon intensity at the sensor due to a star at distance r is given by $\mu(r) = \int_{\lambda_1}^{\lambda_2} I_{\rm D}(\lambda_{\rm D};r){\rm d}\lambda_{\rm D}$. The photon flux arriving from the star to the sensor is therefore $\pi R^2\mu(r)$ where R denotes the sensor radius. The photon flux due to a spherical shell (containing stars) with radius r and width ${\rm d}r$ is $\pi R^2\mu(r){\rm d}N(r)$, where $N(r) = (4\pi/3)\rho_{\rm U}r^3$ is the number of stars inside a spherical cluster of radius r.

The photon intensity at the sensor due to all the other galaxies (except our galaxy) is therefore given by $2\pi\eta_{\rm U} = 1/(4\pi R^2)\int_0^{R_{\rm U}} \pi R^2\mu(r){\rm d}N(r)$. Using the above results, it follows that

$$\eta_{\rm U} = \frac{\rho_{\rm U}}{2}\int_0^{R_{\rm U}} \mu(r)r^2{\rm d}r = \frac{\rho_{\rm U}}{2}\int_0^{R_{\rm U}}\int_{\lambda_1}^{\lambda_2} I_{\rm D}(\lambda;r){\rm d}\lambda r^2{\rm d}r$$
$$= \pi c\rho_{\rm U}R_{\rm S}^2\int_{\lambda_1}^{\lambda_2} \lambda^{-4}J(\lambda_0,R_{\rm U}){\rm d}\lambda.$$

where

$$J(\lambda_0,R_{\rm U}) \triangleq \int_0^{R_{\rm U}} (1+r/R_{\rm U})/\left(e^{(\lambda_0/\lambda)\sqrt{(1+r/R_{\rm U})/(1-r/R_{\rm U})}} - 1\right){\rm d}r.$$

The substitution $y = \sqrt{(1+r/R_{\rm U})/(1-r/R_{\rm U})}$ leads to $J(\lambda_0,R_{\rm U}) = 8R_{\rm U}\int_1^\infty (y^3/(y^2+1)^3)/(e^{(\lambda_0/\lambda)y} - 1){\rm d}y$. Combining this expression and the above results, we get $\eta_{\rm U} = 8\pi c\rho_{\rm U}R_{\rm U}R_{\rm S}^2\int_1^\infty [y^3/(y^2+1)^3]J_1(\lambda_0,y){\rm d}y$, where $J_1(\lambda_0,y) \triangleq \int_{\lambda_1}^{\lambda_2} \lambda^{-4}/[e^{(\lambda_0/\lambda)y} - 1]{\rm d}\lambda$. The substitution $z = (\lambda_0/\lambda)y$ gives $J_1(\lambda_0,y) = (\lambda_0 y)^{-3}\int_{z_2}^{z_1}(z^2/(e^z-1)){\rm d}z$. where $z_1 = (\lambda_0/\lambda_1)y$, $z_2 = (\lambda_0/\lambda_2)y$. The integral for J_1 is therefore expressible in term of the function ϕ as $J_1(\lambda_0,y) = (\lambda_0 y)^{-3}[\phi(\lambda_0 y/\lambda_2) - \phi(\lambda_0 y/\lambda_1)]$. Hence, the final expression for $\eta_{\rm U}$ is $\eta_{\rm U} = 8\pi c\rho_{\rm U}R_{\rm U}R_{\rm S}^2\lambda_0^{-3}\int_1^\infty (\phi(x_2 y) - \phi(x_1 y)/(y^2+1)^3){\rm d}y$, where $x_1 = \lambda_0/\lambda_1$, $x_2 = \lambda_0/\lambda_2$.

As we already found (for $\eta_{\rm G}$ computation) $x_1 = 6$, $x_2 \approx 3.43$. The integral in the last expression for $\eta_{\rm U}$ can be computed numerically approximating the function ϕ in the integrand by its truncated expansion. The approximate numerical value of the integral is 0.01448. Therefore, $\eta_{\rm U} \approx 8\pi c\rho_{\rm U}R_{\rm U}R_{\rm S}^2\lambda_0^{-3} \cdot 0.01448 \approx 6.1 \times 10^{11}\ {\rm s}^{-1}{\rm m}^{-2}{\rm rad}^{-2}$, which gives $\eta_{\rm out} = \eta_{\rm a} + \eta_{\rm G} + \eta_{\rm U} \approx 7.3 \times 10^{11}\ {\rm s}^{-1}{\rm m}^{-2}{\rm rad}^{-2}$. This is the *unattenuated* value of $\eta_{\rm out}$.

Remark A.2: In order to evaluate the attenuated value of $\eta_{\rm out}$, we add to the attenuation of 22 dB due to fog condition an assumed additional attenuation factor of 3 due to clouds, i.e., a total attenuation factor of 37.767. Hence, the *attenuated (practical)* value for $\eta_{\rm out}$ is

$$\eta_{\rm out} \approx 1.9 \times 10^{10}{\rm s}^{-1}{\rm m}^{-2}{\rm rad}^{-2}. \qquad \text{(A.2)}$$

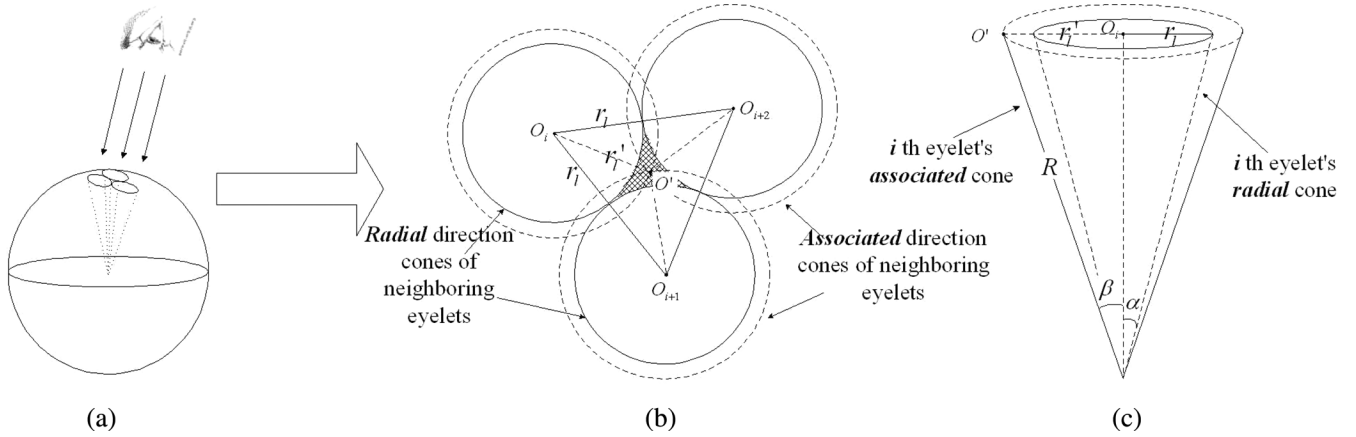

Fig. 6. (a) Top view of three associated cones of source directions of three contiguous eyelets; (b) planar approximation to the top view under large M assumption; and (c) side view of the radial cone and associated cones of the ith eyelet.

APPENDIX B
PROOF OF THEOREM 6.1

Proof:

a) The lower bound on $k_{\rm a}$: We derive the lower limit of the angular expansion factor $k_{\rm a}$, assuming the number of eyelets M is sufficiently large (such that each eyelet's associated cone of source directions is narrow). The lens center points on the surface of the spherical array are determined by the tables in [33].

We consider the associated direction cones of three contiguous identical lenses, namely, the ith, $(i+1)$th, and $(i+2)$th. Fig. 6(a) shows the top view of these cones on the array surface. Under the large M assumption, the edge of the cones (which is a section of the spherical surface) can be approximated by planar circles, as shown in Fig. 6(b), on which each point corresponds to a source direction. Each solid circle represents the radial cone (of source direction) of the corresponding eyelet; the source can be seen from this eyelet *without the lens* if the direction lies in this cone. Each dashed circle represents the associated cone (of source direction) of the eyelet; the source can be detected by this eyelet *with the presence of the lens* if the direction lies in this cone. The centers of the circles are labeled as O_i, O_{i+1}, and O_{i+2}, respectively. The shaded area represents the source direction set which is invisible to the array, since it does not belong to any radial cones.

Obviously, to remove the "blind region" (shaded area), the center of the region (labeled by O') should be enclosed by at least one associated cone under the lens effect. In other words, the "minimal" associated cone should be the dashed circles in Fig. 6(b), which intersect at O'. Clearly, $r_1' = \sqrt{3}/2 r_1$ under the large M assumption (i.e., $\alpha \to 0$), or $\lim_{\alpha\to 0}(r_1'/r_1) = 2/\sqrt{3}$. On the other hand, as shown in Fig. 6(c), generally (i.e., without the large M assumption) $r_1' = R\sin\beta = R\sin(k_{\rm a}\alpha)$ and $r_1 = R\sin\alpha$, where α and β are defined in the figure; i.e., $r_1'/r_1 = \sin(k_{\rm a}\alpha)/\sin\alpha$. It then follows that

$$\frac{2}{\sqrt{3}} = \lim_{\alpha\to 0}\frac{\sin(k_{\rm a}\alpha)}{\sin\alpha} = k_{\rm a}. \tag{B.1}$$

Note that the value of $k_{\rm a}$ in (B.1) is the minimal one that is necessary to remove all the nonvisible regions on the unit sphere surface. Hence, under the large M assumption, $k_{\rm a} \geq (2/\sqrt{3})$, which gives the bound in (6a).

b) The lower bound on σ_x: Let (x, y) be the position of a detected particle on a subarray DS, and $\boldsymbol{p} = [p_x, p_y, p_z]^T$ be the momentum vector of that particle. From the uncertainty principle in quantum mechanics (see, e.g., [29] and [30]), we have

$$\sigma_x \sigma_{p_x} \geq \frac{\hbar}{2} \tag{B.2}$$

where σ_x is the standard deviation of the x component distribution of the detected particles positions on the subarray DS, and σ_{p_x} is the standard deviation of the statistical distribution of the x component of their momenta p_x. Under the azimuthal symmetry assumption, the distributions of positions (x, y) and momenta (p_x, p_y) are azimuth invariant; i.e., $\sigma_x = \sigma_y$ and, similarly, $\sigma_{p_x} = \sigma_{p_y}$. We further assume that σ_x is approximately constant over the DS (this is especially true for a "narrow" eyelet cone of associated directions); thus, the lower bound on σ_x should be achieved at the center of the DS.[8]

It follows from (B.2) that $\sigma_x \geq (\hbar/2\sigma_{p_x})$, where equality is attained (from the derivation of the uncertainty principle using the Cauchy–Schwarz inequality) if and only if the wave function is Gaussian (i.e., x is Gaussian distributed), which indicates that the above lower bound on σ_x may be tight.

Now the problem becomes one of finding an upper bound on σ_{p_x}. Let $P = \sqrt{p_x^2 + p_y^2 + p_z^2}$ denote the norm of the momentum and by $P_{\max}$ its maximal value. We assume that the particle intensity is uniformly distributed over the inner lens surface, so that we may exactly compute the expectation $\mathrm{E}[p_x^2 + p_y^2]$ under this assumption as follows. Let the particle (marginal) probability density at the lens inner surface, on a circle with radius r around the lens symmetry axis be $2\pi r/\pi r_1^2 = 2r/r_1^2$, where the random variable r takes value in the interval $[0, r_1]$. Note that $\int_0^{r_1}(2r/r_1^2)\mathrm{d}r = 1$, which validates the probability density distribution defined above. Hence, $\mathrm{E}[p_x^2 + p_y^2] =$

[8]Even if σ_x fails to be approximately constant over the DS, we still can try to find a lower bound for it in the center of the DS. Then under the assumption that the lens is designed such that σ_x is the smallest at the DS center, this lower bound for σ_x at the DS center still applies to any other point on the DS.

$\mathrm{E}[P^2r^2/(r^2+h_\mathrm{d}^2)] \le P_{\max}^2 \int_0^{r_\mathrm{l}} (r^2/(r^2+h_\mathrm{d}^2))\mathrm{d}(r^2/r_\mathrm{l}^2)$. By changing the integration variable to $x = r^2/r_\mathrm{l}^2$, we get

$$\mathrm{E}\left[p_x^2+p_y^2\right] \le P_{\max}^2 \int_0^1 \frac{x}{x+h_\mathrm{d}^2/r_\mathrm{l}^2}\mathrm{d}x = P_{\max}^2\left[1-\left(\frac{h_\mathrm{d}}{r_\mathrm{l}}\right)^2 \ln\left(1+\left(\frac{r_\mathrm{l}}{h_\mathrm{d}}\right)^2\right)\right].$$

Since $\mathrm{E}[p_x^2+p_y^2] = 2\sigma_{p_x}^2$ by azimuthal symmetry, we see that the lower bound on σ_x is given by

$$\sigma_x \ge \frac{\hbar}{2\sigma_{p_x}} = \frac{\hbar}{\sqrt{2\mathrm{E}\left[p_x^2+p_y^2\right]}} = \frac{\lambda_{\min}}{2\sqrt{2}\pi\sqrt{1-(h_\mathrm{d}/r_\mathrm{l})^2\ln\left[1+(r_\mathrm{l}/h_\mathrm{d})^2\right]}} = \sigma_{x,\mathrm{B}} \quad \text{(B.3)}$$

using the relationship $2\pi\hbar/P_{\max} = \lambda_{\min}$. Note that when $r_\mathrm{l} \ll h_\mathrm{d}$, $\sigma_{x,\mathrm{B}}$ is asymptotically equal to $\lambda_{\min}/2\pi r_\mathrm{l}/h_\mathrm{d})$.

c) The lower bound on σ: According to the relationship $\sigma \simeq k_\mathrm{a}\sigma_x/R_\mathrm{d}$, when σ is sufficiently small, we have the first lower bound on σ:

$$\sigma \ge \frac{k_\mathrm{a}\sigma_{x,\mathrm{B}}}{R_\mathrm{d}} \quad \text{(B.4)}$$

where $\sigma_{x,\mathrm{B}}$ is given in (B.3). In the following we derive the second lower bound on σ corresponding to $\mathrm{MSAE}_{\mathrm{UB}}$.

We assume the particles are arriving independently at the array according to a common LSF, which is responsible for their common angular distribution, assumed to be invariant with respect to the azimuth. Thus, from each detected particle (whose detection may be considered as a single experiment), one may infer the estimated angular distribution of the source direction (i.e., the probability distribution of the possible associated directions that lead to the detection at a specific point) using the LSF. However, from the definition of the LSF, this angular distribution estimate of the source direction (estimated by the lens-shaping function knowledge) should have the same angular distribution as the LSF itself! It follows that the MSAE for the direction of the total momentum of the detected particles is asymptotic to $2\sigma^2/\mathrm{ESC}$ as ESC tends to ∞.

On the other hand, this MSAE has a universal bound where the lens is serving as a "particle sensor" whose cross section has radius r_l instead of R. Hence, according to (8), $2\sigma^2 = \lim_{\mathrm{ESC}\to\infty}[\mathrm{ESC}\cdot\mathrm{MSAE}] \ge \lim_{\mathrm{ESC}\to\infty}[\mathrm{ESC}\cdot\mathrm{MSAE}_{\mathrm{UB}}(R = r_\mathrm{l})] = (x_{0,1}\lambda_{\min}/2\pi r_\mathrm{l})^2$.

It then follows from the above discussion that

$$\sigma \ge \frac{x_{0,1}\lambda_{\min}}{2\sqrt{2}\pi r_\mathrm{l}}. \quad \text{(B.5)}$$

Combining (B.4) and (B.5), we obtain the theoretical lower bound on σ as follows:

$$\sigma \ge \sigma_\mathrm{B} = \max\left\{\frac{k_\mathrm{a}\sigma_{x,\mathrm{B}}}{R_\mathrm{d}}, \frac{x_{0,1}\lambda_{\min}}{2\sqrt{2}\pi r_\mathrm{l}}\right\}. \quad \text{(B.6)}$$

This completes the proof. ■

APPENDIX C
PROOFS OF THEOREMS 7.1 AND 7.2

A. Proof of Theorem 7.1

Proof: In order to prove the theorem, we introduce a definition of a particle detection event as follows.

Definition C.1: A particle is said to be detected inside the sensor detection domain (which is a certain space–time domain), if the presence of a particle inside this domain is observed (i.e., determined) and recorded by the hardware and software of the sensor system.

Definition C.2: A particle-detection event is defined as the first point (x, y, z, t) in space–time where a detected particle started (for the first time) its interaction with the sensor hardware (which leads eventually to its detection.)

Note that prior to its detection, a detected particle behaves as a "free particle" described by a quantum-mechanical wave function, which is a plane wave $\psi(x, y, z, t)$ with expected (free particle) momentum: $\mathrm{E}[\boldsymbol{p}] = \mathrm{E}\{[p_x, p_y, p_z]\} = -i\hbar\langle\nabla\psi, \psi\rangle$, where $\nabla = ((\partial/\partial x), (\partial/\partial y), (\partial/\partial z))$ is the gradient operator. Similarly, the free particle has an expected energy: $\mathrm{E}[E] = i\hbar\langle(\partial\psi/\partial t), \psi\rangle$. To ensure that the sensor software is able to estimate the source direction, $\mathrm{E}[\boldsymbol{p}]$ of the above "free particles" (i.e., prior to their detection event) must be estimated, since $\mathrm{E}[\boldsymbol{p}] = [P_x, P_y, P_z]$ is proportional to $\boldsymbol{u}$ (the source direction) as they carry the same source direction information. Here, we denote

$$\mathrm{E}[p_x] = P_x, \mathrm{E}[p_y] = P_y, \mathrm{E}[p_z] = P_z. \quad \text{(C.1)}$$

Assume that in addition to detecting particles, the sensor is equipped with some software to estimate the momentum $\boldsymbol{p}$ of the particle exactly at its detection event, which leads to a "partial collapse" of the wave function because of the observation act. This is a well known "observation principle" in quantum mechanics in which the modified wave function may be regarded as a result of the former ψ conditioned with respect to the detection and momentum observation.

Note that $\mathrm{E}[\boldsymbol{p}] = [P_x, P_y, P_z]$ for the modified ψ is the same as that of a free particle (since the detection event is just prior to the interaction of the detected particle with the sensor hardware). Hence, due to the conservation of the momentum and energy at the detection event (just before the sensor hardware begins) with respect to that of the free particles, we claim that $\mathrm{E}[\boldsymbol{p}]$ based on the modified ψ (i.e., the wave function describing the particle at the random detection event conditioned on its observation inside the sensor detection domain) is the same $\mathrm{E}[\boldsymbol{p}]$ for the former ψ. Thus, for the modified ψ, we have the following three constraints $\mathrm{E}[\boldsymbol{p}] = [P_x, P_y, P_z]$, where the right-hand-side (RHS) is the same as defined in (C.1) using the former ψ.

Without loss of generality, we may redefine (by rotation) the sensor coordinate frame so that the source direction coincides with the z direction, and we get for the modified ψ: $P_x = P_y = 0$. Also, according to our assumptions, the particle detection event occurs only inside a sensor domain D during a detection time interval $[0, T]$. We denote by D_{ST} the corresponding "detection space-time domain," and denote the quantum wave function of the detected particles inside D_{ST} by $\psi(x, y, z, t)$, which

is a (complex-valued) function in $L^2(\mathbb{R}^4)$ with unit norm; i.e., $\langle\psi,\psi\rangle = 1$.

From a physical viewpoint, ψ is continuous over $\mathbb{R}^4$ and vanishes outside $D_{\rm ST}$ (particularly $\psi = 0$ on $D_{\rm ST}$ boundary). Moreover, ψ is in $C^2[D_{\rm ST}]$ with its derivatives with respect to x, y, z, t in $L^2[\mathbb{R}^4]$ (such that the covariance matrix of its momentum may be well defined).

The momentum components p_x, p_y, p_z of each detected particle are associated (as observables) with the following Hermitian operators on $L^2[\mathbb{R}^4]$: p_x is associated with the operator $-i\hbar(\partial/\partial x)$, and similarly for p_y and p_z with respect to y and z, respectively. Thus, the expectations of p_x and p_x^2 are given by $\mathrm{E}[p_x] = -i\hbar\langle(\partial\psi/\partial x),\psi\rangle$, $\mathrm{E}[p_x^2] = -\hbar^2\langle(\partial^2\psi/\partial x^2),\psi\rangle = \hbar^2\langle(\partial\psi/\partial x),(\partial\psi/\partial x)\rangle$, and its variance is $\mathrm{var}(p_x) = \mathrm{E}[p_x^2] - P_x^2 = \mathrm{E}[p_x^2]$, which follows from the constraint $P_x = 0$. Similar expressions apply for the p_y, p_z components.

For $n \geq 1$, denote by $\mathrm{MSAE}_p(n)$ the MSAE for the direction of the total momentum of detected source particles if *exactly* n particles where detected within the time window. Clearly $\mathrm{MSAE}_p(n)$ is undefined for $n = 0$. For a particle with wavelength λ, the corresponding momentum is $p = h/\lambda$, thus if $\lambda_{\min}$ is the minimal wavelength, then the total momentum of n particles is upper bounded by $nh/\lambda_{\min}$. Therefore

$$\mathrm{MSAE}_p(n) \geq \frac{nE\left[p_x^2 + p_y^2\right]}{(nh/\lambda_{\min})^2}, n \geq 1. \qquad \text{(C.2)}$$

which follows again from the constraints $P_x = P_y = 0$. Note that P_z indicates the direction of source particles before entering the sensor domain D (i.e., the expectation of their momentum component along the direction from the source to the sensor), and ESC is the expected number of source particles entering the sensor domain D during the detection time interval $[0,T]$ (i.e., entering the "detection space-time domain" $D_{\rm ST}$), as defined previously. Clearly $\mathrm{ESC} = \mu a_{\rm cs} T$, where μ is the source particle intensity around the sensor domain D (it is assumed to be uniform there), and $a_{\rm cs}$ is the sensor cross section with respect to the source direction.

Remark C.1: If we denote by D_P the projection of the three-dimensional domain D on the x, y plane, then D_P is a planar domain whose area is $a_{\rm cs}$.

Since both the sensor hardware and the detection wave function ψ (especially inside $D_{\rm ST}$) are unknown in practice, we have to find the minimum for the $\mathrm{MSAE}_{\rm UB}$ in (C.2), which depends (for given P and ESC) only on the wave function ψ, with respect to ψ (subject to the restrictions on ψ).

Thus, we have the constraints $P_x = P_y = 0$, and

$$\begin{aligned}\mathrm{E}\left[p_x^2 + p_y^2\right] &= -\hbar^2\left\langle\left[\left(\frac{\partial}{\partial x}\right)^2 + \left(\frac{\partial}{\partial y}\right)^2\right]\psi,\psi\right\rangle \\ &= \hbar^2\left[\left\langle\frac{\partial\psi}{\partial x},\frac{\partial\psi}{\partial x}\right\rangle + \left\langle\frac{\partial\psi}{\partial y},\frac{\partial\psi}{\partial y}\right\rangle\right]\end{aligned}$$

where the last equality follows from integration by parts. Hence, $\mathrm{MSAE}_p(n) \geq [\lambda_{\min}/(2\pi)]^2 C_{\rm UB} n^{-1}$, where

$$\begin{aligned}C_{\rm UB} = C_{\rm UB}(D_{\rm ST}) &= \inf_f\left[\left\langle\frac{\partial f}{\partial x},\frac{\partial f}{\partial x}\right\rangle + \left\langle\frac{\partial f}{\partial y},\frac{\partial f}{\partial y}\right\rangle\right] \\ &= \inf_f\left[\left\langle -\left[\left(\frac{\partial}{\partial x}\right)^2 + \left(\frac{\partial}{\partial y}\right)^2\right]f, f\right\rangle\right]\end{aligned}$$

in which the infimum is taken over all possible wave functions f in $L^2[\mathbb{R}^4]$ that satisfy the following restrictions: a) $\langle f,f\rangle = 1$; b) f is continuous over $\mathbb{R}^4$ and vanishes outside $D_{\rm ST}$; c) f has first-order derivatives almost everywhere in $D_{\rm ST}$; d) the first-order derivatives of f are in $L^2[\mathbb{R}^4]$; and e) $\langle(\partial f/\partial x), f\rangle = \langle(\partial f/\partial y), f\rangle = 0$, which corresponds to $P_x = P_y = 0$.

Denote by MSAE_p the MSAE of the direction of the total momentum of the detected source particles during the time window *provided* that at least one particle is detected (i.e., $n \geq 1$). Thus, MSAE_p is the expectation of $\mathrm{MSAE}_p(n)$ over *all* positive n values. From the above we get $\mathrm{MSAE}_p \geq [\lambda_{\min}/(2\pi)]^2 C_{\rm UB} E[n^{-1}|n \geq 1]$. The last conditional expectation of n^{-1} over the positive values of n can be estimated from below[9] (after normalization of the Poisson distribution for only positive values of n) with the result $E[n^{-1}|n \geq 1] \geq [1 - e^{-\mathrm{ESC}}]/\mathrm{ESC}$. In addition, it is easy to show that MSAE_0 as defined in Theorem 7.1 is uniformly attained by the MSAE of a random DOA estimator uniformly distributed over the unit sphere, which gives[10] $\mathrm{MSAE}_{\rm av} = \mathrm{MSAE}_0 = \pi^2/2 - 2$ for any estimator whenever $\mathrm{ESC} = 0$. Thus, by Assumption 7.1 and the above discussion we have for any DOA estimator

$$\mathrm{MSAE}(\boldsymbol{u}) \geq \frac{\lambda_{\min}^2 C_{\rm UB}(1 - e^{-\mathrm{ESC}})^2}{(2\pi)^2\mathrm{ESC}} + e^{-\mathrm{ESC}}\mathrm{MSAE}_0(\boldsymbol{u}).$$

To solve the infimum problem for $C_{\rm UB}$, let $D'_{\rm ST}$ be a space-time domain larger than $D_{\rm ST}$ (i.e., containing $D_{\rm ST}$). Clearly, any f satisfying the above restrictions a)–e) in $D_{\rm ST}$ should also satisfy those in $D'_{\rm ST}$. Thus, the above infimum monotonically decreases with increasing D; i.e., $C_{\rm UB}(D'_{\rm ST}) \leq C_{\rm UB}(D_{\rm ST})$, which gives a lower bound for $C_{\rm UB}(D_{\rm ST})$.

We then choose $D'_{\rm ST}$ as the cylindrical domain $D_P \times \mathbb{R}^2$, where (x,y) are restricted to the planar domain D_P and (z,t) are unrestricted. In order to compute $C_{\rm UB}(D'_{\rm ST})$, we use a classical expansion of any function $u(x,y)$ in $L^2(D_P)$ into a Fourier–Bessel orthogonal expansion (see, e.g., [34, Sec. 3.7]) as $u(x,y) = \sum_{m=0}^{\infty}\sum_{n=1}^{\infty} c_{m,n}u_{m,n}(x,y)$, $u_{m,n}(x,y) = J_m(k_{m,n}\rho)e^{im\phi}$, J_m are the Bessel functions with order m, and (ρ,ϕ) is the polar representation of the point (x,y). The parameters $k_{m,n}$ are given by $k_{m,n} = x_{m,n}/R$ where $x_{m,n}$ is the nth positive zero of $J_m(x)$. Note that the selection of $k_{m,n}$ ensures that $u_{m,n}(x,y) = 0$ whenever $\rho = R$; i.e., $x^2 + y^2 = R^2$.

It follows that $u_{m,n}$ are orthogonal in $L^2(D_P)$ and vanish on its boundary.[11] Another well known fact is that the orthogonal sequence $u_{m,n}$ in $L^2(D_P)$ is complete,[12] which justifies the observation that the above expansion of any function $u(x,y)$ in $L^2(D_P)$ should converge in L^2 to $u(x,y)$ itself. Most important, functions $u_{m,n}$ result from the separation of variables method for the 3-D Laplace equation in cylindrical coordinates, which is needed for the following derivation.

It can be easily seen (from, e.g., [34]) that after the z coordinate is separated out, the remaining x, y dependence satisfies

[9]Using Jensen's inequality $\mathrm{E}[n^{-1}|n \geq 1] \geq (\mathrm{E}[n|n \geq 1])^{-1}$.

[10]Using the invariance of MSAE under rotations, and Fubini's Theorem.

[11]E.g., from the orthogonality relations (3.95) in [34].

[12]E.g., w from the theory of Bessel functions.

the following $[(\partial/\partial x)^2+(\partial/\partial y)^2+k^2]u(x,y)=0$, whose solutions are $J_m(k\rho)e^{im\phi}$. Therefore, considering the above restriction (b) that the solutions should vanish on the boundary $\rho=R$, we have $J_m(kR)=0$, which leads to the quantization condition $k=k_{m,n}=x_{m,n}/R$. Thus, for $k=k_{m,n}$ we have

$$\left[\left(\frac{\partial}{\partial x}\right)^2+\left(\frac{\partial}{\partial y}\right)^2+k_{m,n}^2\right]u_{m,n}(x,y)=0. \tag{C.3}$$

Now, letting $f(x,y,z,t)$ be any continuous function in $L^2(\mathbb{R}^4)$ which vanishes whenever $x^2+y^2\geq R^2$, then for any fixed z, t in $\mathbb{R}^2$, we may consider $f(x,y,z,t)$ as an L^2 continuous function of x, y in the disk $x^2+y^2<R^2$ that vanishes outside this disk. Thus, we have by the Fourier–Bessel expansion

$$f(x,y,z,t)=\sum_{m=0}^{\infty}\sum_{n=1}^{\infty}c_{m,n}(z,t)u_{m,n}(x,y) \tag{C.4}$$

where $c_{m,n}(z,t)$ is the appropriate coefficient for this expansion.

Therefore, if f is constrained to have unit norm in $L^2[\mathbb{R}^4]$, i.e., $\langle f,f\rangle=1$, we get

$$\sum_{m=0}^{\infty}\sum_{n=1}^{\infty}\langle c_{m,n},c_{m,n}\rangle\langle u_{m,n},u_{m,n}\rangle=1. \tag{C.5}$$

For "sufficiently regular" f, applying the operator $(\partial/\partial x)^2+(\partial/\partial y)^2$ to the expansion (C.4), we obtain from (C.3)

$$\left[\left(\frac{\partial}{\partial x}\right)^2+\left(\frac{\partial}{\partial y}\right)^2\right]f(x,y,z,t)=\sum_{m=0}^{\infty}\sum_{n=1}^{\infty}-k_{m,n}^2c_{m,n}(z,t)u_{m,n}(x,y).$$

It then follows from integration by parts that

$$\left\langle\frac{\partial f}{\partial x},\frac{\partial f}{\partial x}\right\rangle+\left\langle\frac{\partial f}{\partial y},\frac{\partial f}{\partial y}\right\rangle=\left\langle-\left[\left(\frac{\partial}{\partial x}\right)^2+\left(\frac{\partial}{\partial y}\right)^2\right]f,f\right\rangle=\sum_{m=0}^{\infty}\sum_{n=1}^{\infty}k_{m,n}^2\langle c_{m,n},c_{m,n}\rangle\times\langle u_{m,n},u_{m,n}\rangle.$$

Now, since $k_{m,n}=x_{m,n}/R$ and $x_{m,n}\geq x_{0,1}$ (see e.g., (9.5.2) in [35] for interlacing properties for the zeros of Bessel functions $J_m(x)$), using (C.5) we get the following:

$$\left\langle\frac{\partial f}{\partial x},\frac{\partial f}{\partial x}\right\rangle+\left\langle\frac{\partial f}{\partial y},\frac{\partial f}{\partial y}\right\rangle\geq\left(\frac{x_{0,1}}{R}\right)^2 \tag{C.6}$$

where $x_{0,1}$ is the first positive zero of $J_0(x)$, and its numerical value is approximately 2.40482. The inequality (C.6) is true for sufficiently smooth f and for any f that satisfies the above five constraints a)–e), with the equality attained if and only if the x, y dependence of f is proportional to $u_{0,1}(x,y)$.

Thus, we conclude[13] that $C'_{\mathrm{UB}}=(x_{0,1}/R)^2$. Since $C_{\mathrm{UB}}\geq C'_{\mathrm{UB}}$, we have

$$\mathrm{MSAE}(\boldsymbol{u})\geq\mathrm{MSAE}_{\mathrm{UB}}(1-e^{-\mathrm{ESC}})^2+e^{-\mathrm{ESC}}\mathrm{MSAE}_0(\boldsymbol{u}), \tag{C.7}$$

which implies the result. (The corresponding result for $\mathrm{MSAE}_{\mathrm{av}}(\boldsymbol{u})$ is similarly proved.) ■

B. Proof of Theorem 7.2

Proof: The idea of $\mathrm{MSAE}_{\mathrm{UCR}}$ is to find the wave function $\hat{\psi}(\boldsymbol{p},E)$ describing the momentum-energy probability density of a source particle (instead of the traditional wave function $\psi(x,t)$ describing the space-time probability density); and then to express the resulting CRB and $\mathrm{MSAE}_{\mathrm{CRB}}$ as a function of $\hat{\psi}$, which depends only on the hardware. Therefore, we just need to minimize $\mathrm{MSAE}_{\mathrm{CRB}}(\hat{\psi})$ with respect to any possible $\hat{\psi}$. Furthermore, since the function $\hat{\psi}$ depends very simply on the usual ψ, we need only to minimize $\mathrm{MSAE}_{\mathrm{CRB}}$ with respect to ψ, which will be seen to be trivial.

The connection between $\psi(x,t)$ and $\hat{\psi}(\boldsymbol{p},E)$ can be described as the following. First, note that the space-time (x,t) and the momentum-energy $(\boldsymbol{p},E)$ are dual spaces in the sense that scaling down the space variables $\boldsymbol{x}$ leads to (via the uncertainty principle) scaling up the momentum variables $\boldsymbol{p}$; and vice versa. In other words, the vectors $\boldsymbol{x}$ and $\boldsymbol{p}$ are dual to each other. Similarly, t and E are also dual. A simple guess is that the wave function $\hat{\psi}(\mathrm{p},E)$ is proportional to the Fourier transform of $\psi(x,t)$, where the proportionality constant is determined so that the normalization constraint $\langle\hat{\psi},\hat{\psi}\rangle=1$ is satisfied; i.e., the probability to find the momentum and energy $\boldsymbol{p}$, E of the particle somewhere in the momentum-energy space is 1.

Simple evaluation of the normalization constant shows that the suggested expression for $\hat{\psi}(\mathrm{p},E)$ is given by

$$\hat{\psi}(\boldsymbol{p},E)=h^{-2}\int_{\mathrm{ST}}\psi(x,t)e^{-i(x\cdot\boldsymbol{p}-tE)/\hbar}\mathrm{d}m(x,t) \tag{C.8}$$

where h is Planck's constant, ST denotes the space-time domain, $\hbar$ denotes $h/(2\pi)$ and $\mathrm{d}m(x,t)$ is the standard measure over ST (i.e., over R^4)

Note that i) $\hat{\psi}(\boldsymbol{p},E)$ is proportional to (and may be regarded as) the Fourier transform of $\psi(x,t)$; and ii) since $|\psi(x,t)|^2$ represents the space-time pdf of a particle, it is integrable over ST (i.e., $|\psi|^2$ is in $L^1(R^4)$, or $\psi(x,t)$ is in $L^2(R^4)$).

Since $\hat{\psi}(\mathrm{p},E)$ is the Fourier transform of $\psi(x,t)$, it follows (by Plancherel's theorem) that $\psi(\mathrm{p},E)$ is in $L^2(R^4)$ and by the inversion formula

$$\psi(x,t)=h^{-2}\int_{\mathrm{MES}}\hat{\psi}(\mathrm{p},E)e^{i(x\cdot\boldsymbol{p}-tE)/\hbar}\mathrm{d}m(\mathrm{p},E) \tag{C.9}$$

where MES denotes the momentum-energy space, and $\mathrm{d}m(\mathrm{p},E)$ is the standard measure over MES (i.e., over R^4).

[13]This result is a special case of the classical "Poincaré inequality."

Thus, $\psi(x,t)$ and $\hat{\psi}(\mathrm{p},E)$ are in 1 to 1 correspondence, which is in fact an isometry of $L^2(R^4)$ onto itself—preserving its inner product and norm as an Hilbert space. In particular

$$\langle\psi,\psi\rangle = 1 \qquad \text{if and only if} \qquad \langle\hat{\psi},\hat{\psi}\rangle = 1 \tag{C.10}$$

i.e., the normalization is preserved as desired.

Now, in order to justify our previous "guess" that the above representation of $\hat{\psi}(\boldsymbol{p},E)$ is the correct one, we observe that by applying the operator ∇ to $\psi(x,t)$ (represented by (C.9)) we can get that the operator ∇ in space-time has its dual presentation in momentum-energy as $ip/\hbar$, or

$$\text{the operator p in MES is represented by } -i\hbar\nabla \text{ in ST.} \tag{C.11}$$

Similarly, by applying the time derivative $\partial/\partial t$ operator to $\psi(x,t)$ as represented by (C.9), we get its representation as $-iE/\hbar$ in MES, or

$$\text{the operator E in MES is represented by } i\hbar(\partial/\partial t) \text{ in ST.} \tag{C.12}$$

Repeating applications of these operators, we get that the above representations hold also for all their moments, which is in agreement with the basic quantum-mechanical principles. Since any PDF is uniquely determined by its moments, it follows that the momentum-energy PDF $|\hat{\psi}(\boldsymbol{p},E)|^2$ is uniquely determined by the above guess of $\hat{\psi}(\boldsymbol{p},E)$ given by (C.8). This justifies our guess for the PDF of the momentum-energy over MES, and is all we need to derive the corresponding CRB—the phase of ψ is not needed.

Choosing the z direction of the reference frame to be in the source direction $\boldsymbol{u}$, we evaluate the "partial FIM" corresponding to p_x and p_y components of any particle momentum as what follows. Its components are (using the PDF $f \triangleq |\hat{\psi}(\mathrm{p},E)|^2$) $\mathrm{FIM}(p_x,p_x) = \int_{\mathrm{MES}}((\partial f/\partial p_x)^2/f)\mathrm{d}m(p,E) \leq 4\langle(\partial/\partial p_x)\hat{\psi},(\partial/\partial p_x)\hat{\psi}\rangle$, which can be derived by using the expression for f. Similar expression holds for $\mathrm{FIM}(p_y,p_y)$, hence

$$\mathrm{FIM}(p_x,p_x) \leq 4\left\langle(\partial/\partial p_x)\hat{\psi},(\partial/\partial p_x)\hat{\psi}\right\rangle \tag{C.13}$$

$$\mathrm{FIM}(p_y,p_y) \leq 4\left\langle(\partial/\partial p_y)\hat{\psi},(\partial/\partial p_y)\hat{\psi}\right\rangle. \tag{C.14}$$

Seeing that the corresponding CRB matrix can be found by inverting the FIM, we obtain a lower bound for the $\mathrm{MSAE_{CRB}}$ by using $\mathrm{MSAE_{CRB}} \geq [\mathrm{CRB}(p_x,p_x)+\mathrm{CRB}(p_y,p_y)]/P_{\max}^2$. Thus, $\mathrm{MSAE_{CRB}}$ lower bound is given in terms of $\hat{\psi}$ (which depends of course on the specific hardware used), it is simpler to minimize the $\mathrm{MSAE_{CRB}}$ with respect to the usual ψ instead of the dual $\hat{\psi}$ by observing that

$$\text{the operator } (\partial/\partial p_x) \text{ in MES is represented by } ix/\hbar \text{ in ST.} \tag{C.15}$$

$$\text{the operator } (\partial/\partial p_y) \text{ in MES is represented by } iy/\hbar \text{ in ST.} \tag{C.16}$$

Remark C.2: (C.15) and (C.16) can be proved similar to the proofs of (C.11) and (C.12).

We get from (C.13)–(C.16) [using the normalization (C.10)] $\mathrm{FIM}(p_x,p_x) \leq 4x^2/\hbar^2$, $\mathrm{FIM}(p_y,p_y) \leq 4y^2/\hbar^2$. Thus, from the $\mathrm{MSAE_{CRB}}$ lower bound expression

$$\mathrm{MSAE_{CRB}} \geq \frac{\hbar^2(x^{-2}+y^{-2})}{4P_{\max}^2} \tag{C.17}$$

and $\hbar/P_{\max} = \lambda_{\min}/(2\pi)$, we are led to the minimization problem $\min_{x,y} x^{-2}+y^{-2}$, such that $x^2+y^2=R^2$ because the detection event is inside a sphere of radius R.

It is easy to verify that the minimizer satisfies $x^2 = y^2 = R^2/2$. Inserting this into (C.17), we get $\mathrm{MSAE_{CRB}} \geq (\lambda_{\min}^2/(2\pi R)^2)$. Since this is true for each particle, and since the particles are independent, we finally get (using the expectation of n^{-1} as in the proof of Theorem 7.1)

$$\mathrm{MSAE_{CRB}}(\forall \text{ hardware}) \geq \mathrm{MSAE_{UCR}}[1-e^{-\mathrm{ESC}}]^2 \tag{C.18}$$

which is the result. ■

Appendix D
Concepts, Notations, Assumptions, and Transfer Function Existence for the General Model

We assume that the polarization state of the particles is known (e.g., circular polarization of incoming electromagnetic radiation) in order to simplify the modeling; otherwise, the modeling should be generalized in terms of complex combinations of quantum wave functions corresponding to independent polarization states.

Definition D.1:

a) US—denotes the two-dimensional unit sphere S^2 on which each point $\boldsymbol{u}$ may be regarded as a unit vector representing a direction, and is equipped with its standard (area) measure denoted as $m(\boldsymbol{u})$.
b) EDS—denotes the energy-direction space defined as the (Cartesian) product of $\mathbb{R}_+ = (0,\infty)$ (representing particles energies) with US (representing particles directions). The EDS is equipped with the product measure of the standard measures for $\mathbb{R}_+$ and US, denoted as $m(E,\boldsymbol{u})$. Note that the EDS can also be identified with $\mathbb{R}^3$ without its origin.

Definition D.2:

a) $n(S;p,r;[t_0,t])$—is defined as the *expected* number of (virtual) particles, having their energies and directions in a measurable subset S of the EDS and crossing (both inward and outward) the sphere with center p and radius r during the time window $[t_0,t]$.
b) $I(S;p;[t_0,t])$—is defined as the following limit $\lim_{r\to 0}(n(S;p;r;[t_0,t])/\pi r^2)$ whenever it exists.
c) $I(S;p,t)$—is called the *particle intensity* for a set of energies and directions $S \subset$ EDS at spatial point p and time t, and is defined as the rate with respect to t (whenever it exists) of $I(S;p;[t_0,t])$.

Note that the above definition of $I(S;p,t)$ is *independent* of t_0. This motivates the following assumption.

Assumption D.1: $I(S;p,t)$ exists for every measurable S contained in EDS and every space-time event (p,t). Hence,

$I(S;p,t)$ can be regarded as a distribution (i.e., a positive measure) over the EDS for each given space-time event (p,t).

Note that $I(S;p,t)$ is influenced by the sensor. In order to avoid that effect we introduce the concept of exciting intensity by:

Definition D.3: $\mathrm{EI}(S;p,t)$—is called the *exciting intensity* and defined as the intensity $I(S;p,t)$ *without* the presence of the sensor.

Note that $\mathrm{EI}(S;p,t)$ is *independent* of the sensor presence and not influenced (as $I(S;p,t)$) by its scattering effects.

For simplicity, we assume that the exciting intensity is i) *time-invariant* so that t in the EI notation can be ignored,[14] and ii) is *uniform* in the vicinity of the array due to the far-field source assumption. Accordingly, we denote the time-invariant and uniform EI around the array as $\mathrm{EI}(S)$. Here, we assume that iii) $\mathrm{EI}(S)$, interpreted as an *exciting intensity distribution* over the EDS, is *absolutely continuous* with respect to the standard (product) measure over the EDS. Note that the assumption iii) is physically reasonable since by quantum mechanical principles, the energies and moments of the particles have some joint probability distribution whose density is determined by some wave function.

Definition D.4: $\mu(E,\boldsymbol{u})$—denotes the *EI density* with respect to the standard measure over the EDS, and is defined as the *exciting particle intensity density* at energy E and direction $\boldsymbol{u}$ over the EDS. In practice, we model the contribution of each point-like source to $\mu(E,\boldsymbol{u})$ by a "spherical δ function."

Definition D.5: DS—denotes the *detection surface*, which is defined as any smooth surface tightly enveloping the detectors physical surfaces endowed with its standard area measure.

Let $n(D;S;\mathrm{EI};[t_0,t])$ denote (for any given subset D of DS, subset S of EDS, and EI) the expected particle counts within time window $[t_0,t]$ due to particles hitting D and resulting from the given EI distribution with energies and directions confined to S. Accordingly:

Definition D.6: $\mathrm{DR}(D;S;\mathrm{EI};t)$—denotes the *(time-variant) detection rate* for given subset D of DS, subset S of EDS, and EI, and is defined as the rate with respect to t (whenever it exists) of $n(D;S;\mathrm{EI};[t_0,t])$ at time t.[15] In what follows we assume it to be *time-invariant*, and denote this detection rate by $\mathrm{DR}(D;S;\mathrm{EI})$.

We then make the following assumptions that are needed for the model derivation.

Assumption D.3: (Additivity Assumption of EI and DR With Respect to the EDS): We assume that if S_1 and S_2 are disjoint measurable sets in the EDS with S_3 being their union, then we have $\mathrm{EI}(S_1)+\mathrm{EI}(S_2)=\mathrm{EI}(S_3)$; and for any measurable subset D on the detection surface, $\mathrm{DR}(D;S_1)+\mathrm{DR}(D;S_2)=\mathrm{DR}(D;S_3)$.

Note that this assumption is reasonable for *deterministic* exciting particles, but for *virtual* particles this is not true in general (due to interference effects.) Therefore, we need the following assumption which is a sufficient condition for Assumption D.3.

[14]Time-variant exciting intensities are useful in the modeling of particle communications.

[15]This definition of the detection rate is independent of t_0.

Assumption D.4: Interference effects among exciting particles are *negligible*.

Remark D.1: As examples for Assumption D.4 we may consider a) the *no scatterers* case: in this case the exciting particles are emitted independently of each other; and b) negligible correlations among sources and scatterers: in this case (appearing e.g., in applications with DOA including multipath effects) the correlations among the sources and scatterers (e.g., for EM waves are described by constant phase differences among the vector phasors describing the EM waves from distinct sources and scatterers) are negligible.

Assumption D.5: For any fixed EI and measurable subset D of the DS, the detection rate $\mathrm{DR}(D;S;\mathrm{EI})$—regarded as a positive measure over measurable subsets S of the EDS—is *absolutely continuous* with respect to the positive measure $\mathrm{EI}(S)$ over the EDS. Note that this assumption is physically resonable (since it means that if $\mathrm{EI}(S)=0$ then $\mathrm{DR}(D;S;\mathrm{EI})=0$ as well).

We further define the following.

Definition D.7: $H(D;E,\boldsymbol{u};\mathrm{EI})$—denotes the *detection transfer function* for EI and any given measurable subset D of the DS at point $(E,\boldsymbol{u})$ on the EDS, which is defined as the density of the measure $\mathrm{DR}(D;S;\mathrm{EI})$ with respect to $\mathrm{EI}(S)$. Considering the EI distribution as the sensor "input" and the detection rate distribution as its "output," we can see that $H(D;E,\boldsymbol{u};\mathrm{EI})$ describes the sensor operation by giving its input–output relationship. Note that the existence of the density $H(D;E,\boldsymbol{u};\mathrm{EI})$ is equivalent to assumption D.5.

Now we make more reasonable assumptions (with justifications) in order to simplify the modeling and present parametric structure suitable for analysis. The first step is to make $H(D;E,\boldsymbol{u};\mathrm{EI})$ dependent *only* on the density (assuming its existence) $\mu(E,\boldsymbol{u})$, with value only at $(E,\boldsymbol{u})$ and not the entire distribution EI over the EDS.

Assumption D.6: (Continuity Assumption of $H(D;E,\boldsymbol{u};\mathrm{EI})$ With Respect to E, $\boldsymbol{u}$): We assume that for any given distribution EI and measurable subset D of the DS, the function $H(D;E,\boldsymbol{u};\mathrm{EI})$ as a function of $E,\boldsymbol{u}$ is continuous over the EDS.

Remark D.2: Assumption D.6 is physically reasonable since $H(D;E;\boldsymbol{u};\mathrm{EI})$, as a function of $E,\boldsymbol{u}$, is a result of physical processes described by certain partial differential equations, and as such should be even smooth (and not merely continuous).

Assumption D.7: (Existence and Continuity Assumption of $\mu(E,\boldsymbol{u})$): We assume that each EI distribution over the EDS has a continuous density $\mu(E,\boldsymbol{u})$ with respect to the EDS standard measure.

Remark D.3: The physical validity of Assumption D.7 lies in the fact that since (by the uncertainty principle) the momentum of each particle is distributed, as a result both its energy and direction are distributed as well. Note also that even in classical physics, particle sources are distributed in space (with the only "singular" object—a "black hole"—that cannot emit particles, according to classical physics) and are not truly point-like. However, in this paper we may still use spherical δ distribution for point-like particle sources, but it is only a mathematical idealization of a truly distributed source. The continuity of μ may be physically justified according to Remark D.2. There

is also a mathematical justification to Assumption D.7 in the sense that each EI distribution (as a positive absolutely continuous Borel measure over EDS) can be approximated arbitrarily closely by another distribution with a continuous density $\mu(E,\boldsymbol{u})$. (Moreover, even by infinitely differentiable $\mu(E,\boldsymbol{u})$ with compact support in the EDS—i.e., with finite energy bandwidth—which follows from a well known approximation property of infinitely differentiable functions with compact support in $\mathbb{R}^n$.)

Thus, under Assumptions D.6 and D.7 we have that (for given D and EI) the detection rate $\mathrm{DR}(D;S;\mathrm{EI})$ (as a distribution over the EDS) has a density given by $\lambda(D;E,\boldsymbol{u};\mathrm{EI}) = H(D;E,\boldsymbol{u};\mathrm{EI})\cdot\mu(E,\boldsymbol{u})$. Moreover, by Assumption D.6 and D.7 this density should be continuous with respect to E and $\boldsymbol{u}$. Since $\lambda(D;E,\boldsymbol{u};\mathrm{EI})$ depends (by its definition) only on the *local* properties of the EI around the point $(E,\boldsymbol{u})$, it may depend on EI *only* through $\mu(E,\boldsymbol{u})$ (its value at the specific point $(E,\boldsymbol{u})$ in the EDS). Hence, we may write it as $\lambda(D;E,\boldsymbol{u};\mu(E,\boldsymbol{u}))$ to emphasize this dependence on $\mu(E,\boldsymbol{u})$ (which might be nonlinear in general).

Assumption D.8: We assume that for any fixed D, E, and $\boldsymbol{u}$, the density $\lambda(D;E,\boldsymbol{u};\mu(E,\boldsymbol{u}))$ is a continuous functional of $\mu(E,\boldsymbol{u})$ over $L^1(\mathrm{EDS})$.

The last step to achieve a "truly transfer function" $H(D;E,\boldsymbol{u})$ is to remove the above dependency by assuming:

Assumption D.9: (Weak Intensity Assumption): We assume that the total exciting intensity (TEI) is sufficiently small, such that (according to assumption D.8) we may put $\mu(E,\boldsymbol{u}) = 0$ in $H(D;E,\boldsymbol{u};\mu(E,\boldsymbol{u}))$—making H independent of $\mu(E,\boldsymbol{u})$. Thus, we may write H as $H(D;E,\boldsymbol{u})$—a truly transfer function.

Remark D.4: This assumption merely states that the sensor is working in its "linear zone." For visible light, it is determined mostly by the detectors, instead of the lens and possible optical filters whose operation is approximately linear for higher TEI. More precisely, $H(D;E,\boldsymbol{u};\mathrm{EI}) = H(D;E,\boldsymbol{u}) + o(\mathrm{TEI})$. Note that the above approximation holds (*independently* of the EI distribution) whenever the total intensity $\mathrm{TEI} = \mathrm{EI}(\mathrm{EDS})$ is sufficiently small.

In the following we assume that Assumptions D.3 to D.9 hold so that the transfer function $H(D;E,\boldsymbol{u})$ is well defined. Moreover, we assume that $H(D;E,\boldsymbol{u})$ is sufficiently smooth (e.g., infinitely differentiable)—which is reasonable according to the remark to Assumption D.7.

Definition D.8: $(E_{\mathrm{D}},\boldsymbol{u}_{\mathrm{D}})$—denotes the *associated energies and directions* for each set D (of positive area) on the detection surface, which is defined as the pair $(E,\boldsymbol{u})$ that *maximizes* $H(D;E,\boldsymbol{u})$, assuming existence and uniqueness of the global maximizer. Note that the existence follows from the continuity of H and the reasonable assumption that the transfer function decays to zero as the energy tends to infinity, while the uniqueness is a standard assumption.

Remark D.5: As stated above, the pair $(E_{\mathrm{D}},\boldsymbol{u}_{\mathrm{D}})$ may be calibrated (at least in principle) only in the case where D is a union of detectors.

Remark D.6: The transfer function $H(D;E,\boldsymbol{u})$ is of fundamental importance for the sensor modeling since it contains all the information needed to describe and model the sensor operation. The sensor may be described as an input–output system, whose input is the EI distribution and output is the detection rate $\mathrm{DR}(D)$ distribution over measurable subsets D of the detection surface. Note that the only subsets D for which $\mathrm{DR}(D)$ can be really observed are these which are union of some whole surface of detectors—however, we still have a definition for Borel measurable subsets D.

In order to see that the transfer function H describes completely the behavior of the sensor as an input–output system, we show in the following how to use it to model the sensor operation: let S be any measurable subset of the EDS, we have $\mathrm{DR}(D;S;\mathrm{EI}) = \int_S H(D;E,\boldsymbol{u})\mathrm{dEI}(E,\boldsymbol{u})$, where $\mathrm{dEI}(E,\boldsymbol{u})$ is an element of the exciting particle intensity distribution over the EDS with respect to the $(E,\boldsymbol{u})$ coordinates. Clearly $\mathrm{dEI}(E,\boldsymbol{u}) = \mu(E,\boldsymbol{u})\mathrm{d}m(E,\boldsymbol{u})$, where $\mathrm{d}m(E,\boldsymbol{u})$ is the element of the usual measure over the EDS.

Remark D.7: If d is a detector with E_{d} and $\boldsymbol{u}_{\mathrm{d}}$ as its associated energy and associated direction, then E_{d} and $\boldsymbol{u}_{\mathrm{d}}$ are *observable* and as a result can be *calibrated*. In conclusion, the associated energy and associated direction are defined for any measurable D on the detection surface with *positive* area; while for sets D with zero area, $(E_{\mathrm{D}},\boldsymbol{u}_{\mathrm{D}})$ is defined only when D is a single point (it is not defined e.g., for a one dimensional set like a curve).

Let DS_i denotes the detection surface for the ith eyelet; and *assume* that to each point p on DS_i there is a corresponding direction $\boldsymbol{u}_{\mathrm{p}} = \phi(p)$, where ϕ is a C^2-diffeomorphism from DS_i into US, such that the center of mass (with respect to the standard DS_i measure) for each detector d on DS_i is mapped by ϕ to the associated direction $\boldsymbol{u}_{\mathrm{d}}$ of d. This assumption (about the existence of such ϕ) is reasonable since ϕ, in addition to being smooth, is required to satisfy only a *finite* set of interpolation restrictions. Such ϕ will be called an *interpolating diffeomorphism*. The image $\Omega_{\mathrm{d}} \triangleq \phi(\mathrm{d})$ is called "the cone of associated directions for the detector d," and $\Omega_i \triangleq \phi(\mathrm{DS}_i)$ is called "the cone of associated directions for the ith eyelet" with its *interpolating parametrization* induced by ϕ.

Remark D.8: For each given pair $(E,\boldsymbol{u})$ of the EDS, the transfer function $H(D;E,\boldsymbol{u})$ is a positive measure over the Borel measurable subsets D of the DS, which is absolutely continuous with respect to the solid angle measure of the image $\phi(D)$ of D under the interpolating diffeomorphism ϕ (as described by remark D.7). Therefore, under the assumption that the density of $H(D;E,\boldsymbol{u})$ (as a measure over subsets D) with respect to the solid angle measure of $\phi(D)$ is continuous over D, we get that $H(d;E,\boldsymbol{u})/\Omega_{\mathrm{d}}$ is slowly varying over neighboring detectors. Thus, the transfer function $H(d;E,\boldsymbol{u})$ for each detector d in an eyelet is nearly proportional to the detector's solid angle Ω_{d}. And by redefining the "detector specific transfer function" to be the ratio $H(d;E,\boldsymbol{u})/\Omega_{\mathrm{d}}$ and denoting it again by $H(d;E,\boldsymbol{u})$, we get that $H(d;E,\boldsymbol{u})$ is almost independent of the detector d (irrespective of its solid angle Ω_{d}); then from remark D.6, we have

$$\mathrm{DR}(d;\mathrm{EI}) = \Omega_{\mathrm{d}} \int_{\mathrm{EDS}} H(d;E,\boldsymbol{u})\mu(E,\boldsymbol{u})\mathrm{d}m(E,\boldsymbol{u}).$$

For the detection rate for each detector d due to the density $\mu(E,\boldsymbol{u})$ of the exciting particle intensity distribution EI over the

EDS. Similar assumption exists for the noisy count rate for each detector, which should be nearly proportional to the detector's solid angle $\Omega_{\rm d}$ of its cone of associated directions.

Definition D.9: To each point p on the DS, there correspond its "radial direction" $\boldsymbol{v}_{\rm p}$ defined as the unit vector in the direction of the radius vector from the spherical array center to p. For each measurable subset D of the DS, denote by $\boldsymbol{v}_{\rm D}$ its "cone of radial directions" which consists the radial directions $\boldsymbol{v}_{\rm p}$ for all points p in D. Clearly, this induces a "radial diffeomorphism" ϕ_R from DS into US by $\phi_R(p) = v_{\rm p}$ for each point p on the DS, whose restriction to D is a diffeomorphism from D *onto* $\phi_R(D) = \boldsymbol{v}_{\rm D}$. By Remark D.7, there is another diffeomorphism ϕ from the DS into the US sending each point p on the DS to its associate direction $\boldsymbol{u}_{\rm p}$. The Jacobian of the transformation from the radial directions $\phi_R(p) = \boldsymbol{v}_{\rm p}$ to the associated directions $\phi(p) = \boldsymbol{u}_{\rm p}$ (for any point p on the DS) is called "solid angle expansion factor" with its square root called "angular expansion factor" and denoted by $k_{\rm a}$. Note that though $k_{\rm a}$ is defined locally and may vary over the DS, for eyelets with sufficiently small angular aperture, we may assume $k_{\rm a}$ to be (nearly) constant over the eyelet's associated cone of directions. The physical explanation for the angular expansion factor is mainly due to the lens focusing effect.

Appendix E
Spherical Gaussian Functions, PG Functions, and LPG Functions

A spherical Gaussian function (of a unit vector $\boldsymbol{u}$) over the US is defined to be proportional to $e^{-Q(\boldsymbol{u}-\boldsymbol{u}_0)}$ where $\boldsymbol{u}_0$ is a fixed unit vector, and $Q(\boldsymbol{u}-\boldsymbol{u}_0)$ is positive-semi-definite (PSD) quadratic form in the components of $\boldsymbol{u}-\boldsymbol{u}_0$. More specifically, we denote (up to a normalization factor) by $\mathcal{N}(\boldsymbol{u};\boldsymbol{u}_0,P)$ the function $e^{-(1/2)(\boldsymbol{u}-\boldsymbol{u}_0)^T P^{-1}(\boldsymbol{u}-\boldsymbol{u}_0)}$, where $\boldsymbol{u}_0$ is a unit vector (the mean) and P is a positive definite 3×3 matrix (the covariance). Given any 2-dimensional local parametrization of $\boldsymbol{u}$ in a neighborhood of $\boldsymbol{u}_0$ (i.e., parametrization of the 2-dimensional component of $\boldsymbol{u}$ that is orthogonal to $\boldsymbol{u}_0$), $\mathcal{N}(u;u_o,P)$ has a *local* 2×2 covariance matrix at $\boldsymbol{u}_0$ with respect to any given such parametrization, defined as the inverse of the Hessian at $\boldsymbol{u}_0$ (with respect to the given local parametrization) of $-\log\mathcal{N}(\boldsymbol{u};\boldsymbol{u}_0,P)$. Note that any sufficiently smooth function $f(\boldsymbol{u})$ over the US with a local maximum at $\boldsymbol{u}_0$, can be approximated locally near $\boldsymbol{u}_0$ (up to second order Taylor expansion terms) by a suitable spherical Gaussian function whose 2×2 local covariance at $\boldsymbol{u}_0$ agrees with the local covariance of $f(\boldsymbol{u})$ at $\boldsymbol{u}_0$ (i.e., the inverse of the Hessian at $\boldsymbol{u}_0$ of $-\log f(\boldsymbol{u})$).

Note that for $P=\sigma^2 I_3$ we get a circular Gaussian function on the US, which is invariant with respect to the choice of reference frame. The normalization constant in this case is $(1/2\pi\sigma^2)[1-e^{-2/\sigma^2}]^{-1}$. However, it is customary to define it as $1/(2\pi\sigma^2)$ because its relative error is negligible for practical values of σ.

A spherical polynomial $p(\boldsymbol{u})$ over the US is a polynomial in the components of the unit vector $\boldsymbol{u}$. It is well known (e.g., from the properties of the spherical harmonics) that each continuous function on the US is *uniformly* approximable arbitrarily closely by spherical polynomials.

A PG function over the US is defined as a spherical polynomial multiplied by a spherical Gaussian function. Obviously, any continuous function on the US is uniformly approximable arbitrarily closely by PG functions.

LPG functions are linear combinations of PG functions and are very suitable for approximating sufficiently smooth functions with several maxima over the US. The method is to select certain "important" peaks of the given function and to approximate it in a neighborhood of the peak by a Gaussian function whose mean and local covariance at the peak is adapted to that of the given function, then the approximating LPG function is found as a linear combination of each Gaussian function multiplied by a suitable spherical polynomial of bounded order so as to minimize this approximating error in $L^2(\mathrm{US})$ sense. This gives a standard LS optimization for the LPG function coefficients.

References

[1] K. Kleinknecht, *Detectors for Particle Radiation*. Cambridge, U.K.: Cambridge Univ. Press, 1986.

[2] G. F. Knoll, *Radiation Detection and Measurement*, 2nd ed. New York: Wiley, Jan. 2000.

[3] R. H. Kingston, *Detection of Optical and Infrared Radiation*. Berlin, Germany: Springer-Verlag, 1978.

[4] R. W. Boyd, *Radiometry and the Detection of Optical Radiation*, 2nd ed. New York: Wiley, 1983.

[5] A. Nehorai and E. Paldi, "Localization of particle sources with detector arrays," in *Conf. Rec. 27th Asilomar Conf. Signals, Systems, Computers*, Nov. 1993, vol. 2, pp. 981–985.

[6] Z. Liu and A. Nehorai, "Detection of particle sources with directional detector arrays and a mean-difference test," *IEEE Trans. Signal Process.*, vol. 53, no. 12, pp. 4472–4484, Dec. 2005.

[7] Z. Liu, A. Nehorai, and E. Paldi, "Statistical analysis of a generalized compound eye detector array," in *Proc. 4th IEEE Sensor Conf.*, Irvine, CA, Oct. 30–Nov. 2, 2005, 4 pp..

[8] A. Nehorai, Z. Liu, and E. Paldi, "Optimal design of a generalized compound eye particle detector array," in *Proc. SPIE Intelligent Integrated Microsystems*, Orlando, FL, Apr. 2006, vol. 6232.

[9] N. Franceschini, J. M. Pichon, and C. Blanes, "From insect vision to robot vision," *Philos. Trans. Roy. Soc. London B, Biol. Sci.*, vol. 337, pp. 283–294, 1992.

[10] K.-H. Jeong, J. Kim, and L. P. Lee, "Biologically inspired artificial compound eyes," *Science*, vol. 312, pp. 557–561, Apr. 2006.

[11] S. Exner, *The Physiology of the Compound Eyes of Insects and Crustaceans* Transl.: R. C. Hardie, 1989 ed. Berlin, Germany: Springer, 1891.

[12] D.-E. Nilsson, "Optics and evolution of the compound eye," in *Facets of Vision*, D. G. Stavenga and R. C. Hardie, Eds. Berlin, Germany: Springer-Verlag, 1989.

[13] M. F. Land, "Microlens arrays in the animal kingdom," *J. Eur. Opt. Soc. Part A, Pure Appl. Opt.*, vol. 6, no. 6, pp. 599–602, 1997.

[14] D. Porter and D. S. G. Stirling, *Integral Equations, A Practical Treatment, From Spectral Theory to Applications*. Cambridge, U.K.: Cambridge Univ. Press, 1990.

[15] C. R. MacCluer, "The many proofs and applications of perron's theorem," *SIAM Rev.*, vol. 42, no. 3, pp. 487–498, 2000.

[16] M. D. Shuster, "A survey of attitude representations," *J. Astronaut. Sci.*, vol. 41, pp. 439–517, Oct.–Dec. 1993.

[17] P. Hall and P. Qiu, "Nonparametric estimation of a point-spread function in multivariate problems," *Ann. Statist.* [Online]. Available: http://www.stat.umn.edu/~qiu/research/psf1.pdf, to be published

[18] Y. Zhang and A. Roorda, "Evaluating the lateral resolution of the adaptive optics scanning laser ophthalmoscope," *J. Biomed. Opt.*, vol. 11, no. 1, p. 014002, Jan./Feb. 2006.

[19] K. J. Mighell, "A theoretical photometric and astrometric performance model for point spread function CCD stellar photometry," in *Astronomical Data Analysis Software Systems XII, ASP Conf. Series*, 2003, vol. 295, pp. 395–398.

[20] A. W. Clegg, A. L. Feya, and T. J. W. Lazio, "The Gaussian plasma lens in astrophysics: Refraction," *Astrophys. J.*, vol. 496, pp. 253–266, 1998.

[21] J. Tunstall and G. A. Horridge, "Electrophysiological investigation of the optics of the locust retina," *Z. Vergl. Physiol.*, vol. 55, p. 167, 1967.
[22] M. J. Tovée, *An Introduction to the Visual System*. Cambridge, U.K.: Cambridge Univ. Press, 1996.
[23] M. Planck, "On the law of distribution of energy in the normal spectrum," *Ann. Phys. (Germany)*, vol. 4, p. 553, 1901.
[24] E. Hecht, *Optics*, 2nd ed. Reading, MA: Addison-Wesley, 1987.
[25] A. Nehorai and E. Paldi, "Vector-sensor array processing for electromagnetic source localization," *IEEE Trans. Signal Process.*, vol. 42, no. 2, pp. 376–398, Feb. 1994.
[26] A. Nehorai and M. Hawkes, "Performance bounds for estimating vector systems," *IEEE Trans. Signal Process.*, vol. 48, no. 6, pp. 1737–1749, Jun. 2000.
[27] P. E. Caines, *Linear Stochastic Systems*. New York: Wiley, 1988.
[28] Z. Liu, A. Nehorai, and E. Paldi, "A biologically inspired compound eye detector array—Part II: Statistical performance analysis," *IEEE Trans. Signal Process.*, vol. 57, no. 5, May 2009.
[29] S. S. Goh and C. A. Micchelli, "Uncertainty principles in Hilbert spaces," *J. Fourier Anal. Appl.*, vol. 8, no. 4, pp. 335–373, 2002.
[30] E. Breitenberger, "Uncertainty measures and uncertainty relations for angle observables," *Found. Phys.*, vol. 15, no. 3, pp. 353–364, 1985.
[31] G. Elert, Temperature of a Candle Flame. [Online]. Available: http://hypertextbook.com/facts/1999/JaneFishler.shtml
[32] J. N. Bahcall, "Star counts and galactic structure," *Annu. Rev. Astron. Astrophys.*, vol. 24, pp. 577–611.
[33] R. H. Hardin, N. J. A. Sloane, and W. D. Smith, Tables of Spherical Codes With Icosahedral Symmetry. [Online]. Available: http://www.research.att.com/~njas/icosahedral.codes/index.html
[34] J. D. Jackson, *Classical Electrodynamics*, 3rd ed. New York: Wiley, 1991.
[35] M. Abramowitz and I. A. Stegun, *Handbook of Mathematical Functions With Formulas, Graphs, and Mathematical Tables*. New York: Dover, 1972.

Zhi Liu (S'04) received the Ph.D. degree in electrical and system engineering from Washington University in St. Louis in 2007, the M.Sc. degree in information and control engineering from Tongji University, China, in 2001, and the B.Sc. degree in electrical engineering from the North China University of Technology (NCUT), Beijing, China, in 1996.

Since 2007, he has been a Software Developer with OSISoft INC., San Leandro, CA. His current work includes implementing signal processing techniques in the development of data acquiring and processing software. His research interests focus on statistical signal processing and its biologically inspired application to sensor-array processing. He is also interested in image processing, medical imaging (e.g., PET and SPECT), and biological vision.

Dr. Liu has been a member of the Phi Kappa Phi honor society by election since April 2004. He received the Siemens Prize for outstanding graduate study in 2000.

Arye Nehorai (S'80–M'83–SM'90–F'94) received the B.Sc. and M.Sc. degrees in electrical engineering from the Technion—Israel Institute of Technology, Haifa, Israel, and the Ph.D. degree in electrical engineering from Stanford University, Stanford, CA.

From 1985 to 1995, he was a Faculty Member with the Department of Electrical Engineering at Yale University. In 1995, he became a Full Professor the Department of Electrical Engineering and Computer Science at The University of Illinois at Chicago (UIC). From 2000 to 2001, he was Chair of the department's Electrical and Computer Engineering (ECE) Division, which then became a new department. In 2001, he was named University Scholar of the University of Illinois. In 2006, he became Chairman of the Department of Electrical and Systems Engineering at Washington University in St. Louis. He is the inaugural holder of the Eugene and Martha Lohman Professorship and the Director of the Center for Sensor Signal and Information Processing (CSSIP) at WUSTL since 2006.

Dr. Nehorai was Editor-in-Chief of the IEEE TRANSACTIONS ON SIGNAL PROCESSING from 2000 to 2002. From 2003 to 2005, he was Vice President (Publications) of the IEEE Signal Processing Society (SPS), Chair of the Publications Board, member of the Board of Governors, and member of the Executive Committee of this Society. From 2003 to 2006, he was the founding editor of the special columns on Leadership Reflections in the *IEEE Signal Processing Magazine*. He was corecipient of the IEEE SPS 1989 Senior Award for Best Paper with P. Stoica, coauthor of the 2003 Young Author Best Paper Award and corecipient of the 2004 Magazine Paper Award with A. Dogandzic. He was elected Distinguished Lecturer of the IEEE SPS for the term 2004 to 2005 and received the 2006 IEEE SPS Technical Achievement Award. He is the Principal Investigator of the new multidisciplinary university research initiative (MURI) project entitled Adaptive Waveform Diversity for Full Spectral Dominance. He has been a Fellow of the Royal Statistical Society since 1996.

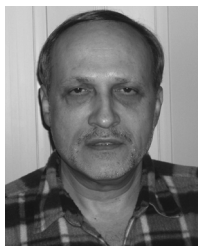

Eytan Paldi (S'87–M'94) received the B.Sc. and M.Sc. degrees in mathematics and the B.Sc. and D.Sc. degrees in electrical engineering from the Technion—Israel Institute of Technology, Haifa, in 1977, 1984, 1978, and 1990, respectively. He is currently working towards the Ph.D. degree in mathematics at the Technion.

From 1979 to 1986, he was a Mathematician and Software Engineer with Elbit Computers, Inc., working on R&D projects in avionics. From 1986 to 1990, he was a Teaching Assistant at the Technion. From 1990 to 1991, he was an HTI postdoctoral Fellow, and from 1991 to 1993 he was a Postdoctoral Associate with the Department of Electrical Engineering at Yale University, New Haven, CT. In 1994, he worked on a mathematical research and development project at IBM, Haifa, Israel. Since 1995, he is an independent scientific consultant for industrial research and development projects. His current research interests are in stochastic modeling, estimation, optimization, polynomial root clustering, rational non-negative definite kernels, and conformal surgery methods in complex analysis.

Dr. Paldi was awarded, during his studies, several Gutwirth Fellowships, the Jury Prize, and the Kennedy-Leigh Prize.